Quaternary Science Reviews 372 (2026) 109727

Contents lists available at ScienceDirect

Quaternary Science Reviews

journal homepage: www.elsevier.com/locate/quascirev

A comparison of Holocene temperature reconstructions from vegetation proxies and brGDGTs in northern Fennoscandia

Liva Trasune[a,*,1], Lilia E. Orozco[b,1], J. Sakari Salonen[a], Gerard A. Otiniano[c,d], Trevor J. Porter[c], Jan Weckström[b], Michael A. Phillips[e,f], Frederik Schenk[a,g,h], Maija Heikkilä[b,i]

[a] Department of Geosciences and Geography, University of Helsinki, Helsinki, Finland
[b] Faculty of Biological and Environmental Sciences, University of Helsinki, Finland
[c] Department of Geography, Geomatics and Environment, University of Toronto - Mississauga, Mississauga, Canada
[d] Department of Earth Sciences, University at Buffalo, Buffalo, NY, USA
[e] Department of Biology, University of Toronto - Mississauga, Mississauga, Canada
[f] Department of Cell and Systems Biology, University of Toronto, Toronto, Canada
[g] Bolin Centre for Climate Research, Stockholm University, Stockholm, Sweden
[h] Department of Geological Sciences, Stockholm University, Stockholm, Sweden
[i] Environmental Change, Geological Survey of Finland, Espoo, Finland

ARTICLE INFO

Handling Editor: Dr P Rioual

Keywords:
Paleoclimatology
Pollen
Plant macrofossils
brGDGTs
Holocene
Europe
Fennoscandia
Vegetation dynamics
Climate reconstruction

ABSTRACT

Studies on Holocene climate conditions commonly show discrepancies between different proxy-based reconstructions, calling for in-depth analysis of both the proxies and the derived climate reconstructions. Here, we conducted multi-proxy Holocene warm-season temperature reconstructions for a sedimentary record from Lake Tippakuru in northeastern Finland, using pollen, plant macrofossils, and the novel branched glycerol dialkyl glycerol tetraethers (brGDGTs) as climate proxies. In addition, we prepared a regional climate reconstruction by integrating pollen-based reconstructions from nearby sites. Mainly, we evaluated the potential of using brGDGTs as a climate proxy and compared the reconstructed climate shifts with those reconstructed from classical vegetation-based proxies (pollen and plant macrofossils). We see significant discrepancies between the three proxies, most notably during the early Holocene where plant macrofossils and brGDGTs indicate warm conditions while the pollen-based reconstructions are equivocal and strongly depend on the quantitative reconstruction method used. Additionally, the brGDGT records indicate an abrupt cooling at ca. 5.8 cal ka BP which is not seen in the classical proxies at the study site, but only in neighbouring localities. The results highlight the need for modern-day studies on seasonal variability and bacterial sources of brGDGTs to disentangle non-thermal biases and evaluate seasonal imprints in temperature reconstructions. In general, our results imply that not only the choice of climate proxies but also the methodological choices in the proxy-based quantitative reconstructions affect the climatic interpretation, especially during the early Holocene transitional period. We highlight the need for both multi-proxy and multi-method approaches in paleoclimate studies, as well as the need to expand the knowledge of brGDGT responses to climatic and other environmental variables.

1. Introduction

The Holocene is a time period known for its long-term shifts in climatic conditions, driven by shifts in insolation patterns and climate system feedbacks (Laskar et al., 2004; Miller et al., 2010; Bradley, 2014). Additionally, the general Holocene climate trends were interrupted by short-term climate shifts, such as the well-known 8.2 ka cold and dry event (Alley et al., 1997; Bond et al., 1997; Clark et al., 2001; Alley and Agustsdottir, 2005), linked to disturbances in North Atlantic thermohaline circulation patterns. These long-term climate trends and abrupt climate anomalies have, in turn, greatly shaped the characteristics of local and regional vegetation and environments.

---

* Corresponding author.
E-mail address: liva.trasune@helsinki.fi (L. Trasune).

[1] shared first author.

https://doi.org/10.1016/j.quascirev.2025.109727
Received 28 August 2025; Received in revised form 24 November 2025; Accepted 24 November 2025

Understanding the intensity and timing of Holocene climate variability at local to regional scales across northern Europe and the circum-Arctic remains the subject of ongoing paleoclimate research (Seppä et al., 2008, 2009; Sejrup et al., 2016; Kaufman et al., 2020). For example, the timing of the well-recorded Holocene Thermal Maximum (HTM), the warmest stage of the interglacial, varies regionally (Renssen et al., 2009, 2012). In northern Finland and nearby regions, climate reconstructions suggest the start of the HTM somewhere between ca. 6 cal ka BP (Shala et al., 2017; Otiniano et al., 2024; Salonen et al., 2024) and ca. 8 cal ka BP (Seppä et al., 2009; Lenz et al., 2021; Krikunova et al., 2022). Such discrepancies could be explained by uncertainties in the quantitative methods used (Birks et al., 2011; Juggins and Birks, 2012), non-climatic drivers impacting the ecology of bioindicators (Väliranta et al., 2015), or between-site differences in fossil datasets resulting from local taphonomic processes (Salonen et al., 2024). Local environmental proxies (plant macrofossils and chironomids), for example, indicate an early start of the Holocene warming, while terrestrial pollen records may exhibit delayed response to environmental shifts (Webb, 1986; Väliranta et al., 2015; Shala et al., 2017). Thus, a temperature proxy not based on micro- or macrofossil assemblages, such as branched (br-)glycerol dialkyl glycerol tetraethers (GDGTs), can give a valuable complementary perspective on past warm-season temperature trends (Pearson et al., 2011; Weijers et al., 2007; De Jonge et al., 2014). BrGDGTs are a molecular fossil from the membrane lipids of bacteria that are ubiquitous in terrestrial and aquatic ecosystems (Damsté et al., 2009; Schouten et al., 2013; Weijers et al., 2006), and, thus, they have an inherent potential to provide novel paleoclimatic insights where they are preserved in the geologic record. Lacustrine brGDGT indices have been used to represent the average lake temperature of the months above freezing (MAF, period from May to September), which broadly aligns with a warm-season temperature signal (Cao et al., 2020) while also being consistent with evidence for enhanced brGDGT production during the fall and winter (Loomis et al., 2014). Furthermore, brGDGTs can be extracted alongside other membrane lipids, and their analysis is faster compared to other biological proxies that involve a laborious process of microscopic species identification. Including the brGDGT temperature proxy brings a new perspective to understanding the nuances of past climate trends and events compared to the classical vegetation-based proxies. Properly validated, brGDGTs could then provide a significant volume of complementary proxy data for regional and global paleoclimate synthesis, which in land areas continues to heavily draw on pollen and other microfossil data (Kaufman et al., 2020).

In this study, we aim to test and compare brGDGTs as climate indicators in relation to novel probability-based plant macrofossil reconstruction algorithms and classical pollen proxy by assessing the differences in timing and intensity of the Holocene events in northern Finland. We reconstruct the mean July air temperature (T_{jul}) using pollen and plant macrofossils and the mean temperature of MAF (T_{MAF}) using brGDGTs from Lake Tippakuru in northeastern Finland. Additionally, we integrate high-resolution pollen-based temperature reconstructions from nearby sites – Lake Loitsana (Shala et al., 2017) and Lake Kuutsjärvi (Salonen et al., 2024) – to investigate the spatial coherence of Holocene temperature patterns and taphonomic influences on pollen-based temperature reconstructions in northern Finland.

2. Materials and methods

2.1. Study site

Lake Tippakuru (67°46′N 29°37′E; 280 m a.s.l.; 5 m maximum depth; 0.2 ha surface area) is a small headwater lake in northeastern Finland, inside the Värriö strict nature reserve (Fig. 1). The catchment consists of sparse northern boreal forest, dominated by Scots pine (*Pinus sylvestris*) and Norway spruce (*Picea abies*). The region has a subarctic climate with the mean annual air temperature (MAAT) of 0 ± 1 °C, T_{jul} of 13 ± 3 °C, T_{MAF} of 9 ± 4 °C, and a total annual precipitation of 566 ± 84 mm for the normal period 1991–2020 CE (Common Era) (Salla Värriötunturi meteorological station 67°44′N 29°36′E) (Finnish Meteorological Institute, 2024). At present, the lake is meso-oligotrophic with clear water (total P 5–13 μg l^{-1}, total N 100–450 μg $\mathrm{l}^{-1,}$ and Secchi depth of 4.5 m) and supports abundant aquatic mosses and benthic algal mats.

2.2. Coring and sampling

We cored Lake Tippakuru from the ice in March 2022 in the deep basin (water depth ∼ 5 m) with a Russian-type peat corer (Jowsey,

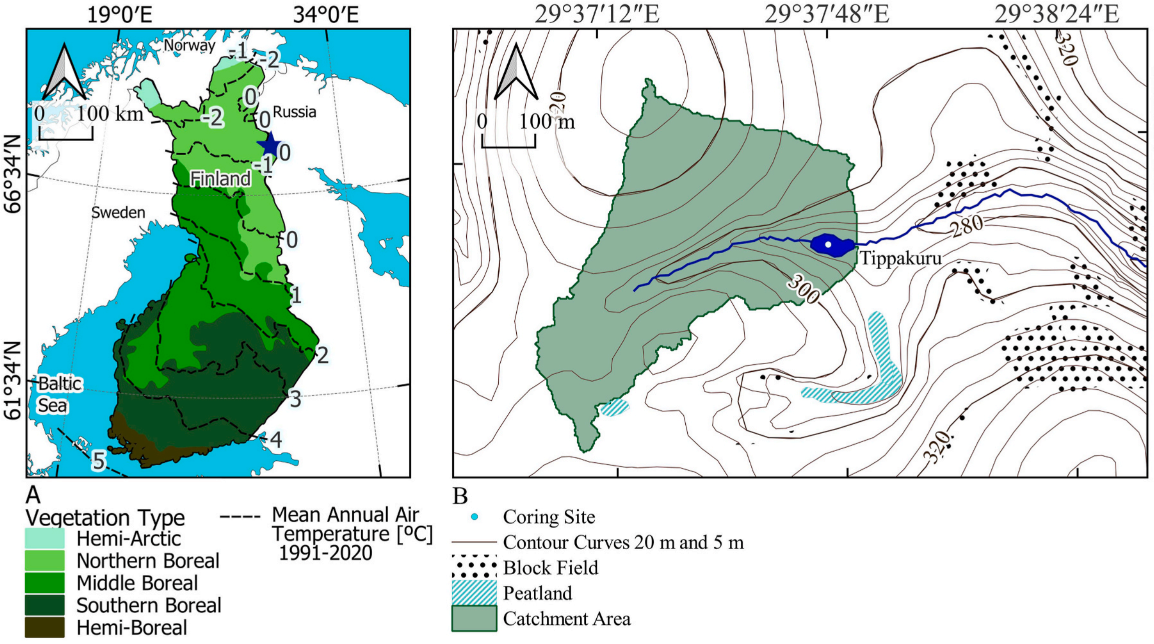

Fig. 1. Study site. **A:** geographical location of Lake Tippakuru with the vegetation zones (Finnish Environmental Center, 2020), and MAAT for the normal period 1991–2020 (Finnish Meteorological Institute, 2022). **B:** Lake Tippakuru and its catchment area calculated from the Digital elevation model 2 m (National Land Survey of Finland, 2014) using GrassGIS 8.3 (GRASS Development Team, 2024).

1966). The total sediment sequence of 3.11 m consists of five parallel, partly overlapping cores of 75 cm to 1 m in length. We subsampled the sediment cores into 1-cm-thick slices and stored them at 4 °C until further analyses at the University of Helsinki. We correlated the cores using the moisture content and organic matter content from loss-on-ignition (LOI; Heiri et al., 2001). For LOI, 2-g subsamples at 1 cm interval within overlapping core depths, and at 4-cm intervals for the rest of the sequence, were dried at 107 °C in an automated furnace until a constant weight was reached and then combusted at 550 °C until at constant weight (SFS-3008 standardized protocol), using LECO TGA701 Thermogravimetric Analyzer at the Environmental Laboratory in the University of Helsinki. The OM content was calculated as:

$$OM_{\%} = \frac{DW_{107} - DW_{505}}{DW_{107}} * 100\ldots \qquad \text{Eq.1}$$

The OM is the calculated organic matter in percentage, and DW is the weight of each sample after drying (DW_{107}) and combustion (DW_{550}).

2.3. Chronology

A total of 34 samples, including 30 macroscopic plant remains and four freeze-dried gyttja samples, were radiocarbon (^{14}C) dated using accelerator-mass-spectrometry (AMS) at the Poznań radiocarbon laboratory, Poland (Table S1). This sampling strategy results in 2–3 dates per millennium on average, thus reaching the minimum recommended dating density of two dates per millennium for a reasonable age-depth model to assess centennial-scale fluctuations (Blaauw et al., 2018). The acquired conventional radiocarbon ages were calibrated using the IntCal20 calibration curve (Reimer et al., 2020) and expressed in calibrated kiloyears before present (cal ka BP). We prepared a Bayesian age-depth model using the library *rbacon* (version 3.1.1; Blaauw and Christen, 2011) in R version 4.3.3 (R Core Team, 2023). For the age-depth modelling, we used a model section thickness of two cm, accumulation shape of two, accumulation rate of 20, and Markov Chain Monte Carlo (MCMC) iteration size of 4000.

2.4. Pollen and plant macrofossil analyses

We prepared pollen samples from 1 cm^3 subsamples, using HCl, KOH, sieving (212 μm mesh), acetolysis, and bromoform heavy-liquid treatments, and mounted them in glycerol. We counted a total of 93 pollen samples, mostly at 4 cm intervals, but with resolution doubled to 2 cm for the uppermost 44 cm to recover a high-resolution pollen dataset for the late Holocene which was covered at only low resolution in earlier pollen sequences analyzed from the nearby Lake Loitsana (Salonen et al., 2013) and Lake Kuutsjärvi (Salonen et al., 2024). We counted a mean of 613 (min = 461, max = 742) terrestrial pollen and spore grains from each sample. Pollen and spores were identified according to Moore et al. (1991) and Reille (1992) and stomata – according to Sweeney (2004).

We conducted plant macrofossil analysis according to procedures described by Birks (2002). After subsampling for other analyses, we wet-sieved all the remaining material using 125 μm mesh under running tap water and stored it until further analysis. Using a stereomicroscope at the University of Helsinki, we analyzed every second centimeter of the core, amounting to 156 samples with volumes ranging from 1 to 20.5 ml. During the plant macrofossil analysis, we also recorded other remains we encountered, including non-plant organisms, sand and charcoal particles. A systematic analysis for those, however, is yet to be conducted. We identified the remains according to Berggren (1981), Birks (2013), Cañellas-Boltà et al. (2012), Cappers et al. (2012), Mauquoy and Van Geel (2013), and Sheinkman et al. (2016).

2.5. brGDGTs extraction and characterization

We extracted and purified brGDGTs from approximately 2 g of freeze-dried sediments at an average interval of 4 cm following previous protocols (Bakkelund et al., 2018; Muñoz et al., 2020) at the University of Toronto - Mississauga campus. We separated the fossil lipids from the sediments by repeated solvent extraction with a 9:1 dichloromethane (DCM)/methanol (MeOH) solution in an Ethos Up Microwave at 70 °C with a magnetic stirrer. The total lipid extract was split into two fractions by column chromatography over an aminopropyl silyl-gel stationary phase: (1) a GDGT fraction eluted with a 2:1 dichloromethane/isopropanol mobile phase; and (2) a high-polarity fraction eluted with 4 % formic acid in diethyl ether. The high-polarity fraction was collected for a separate study and is not discussed here. The GDGT fraction was analyzed with a Agilent Technologies 1290 Series II Ultra High Performance Chromatograph coupled to an AM Sciex 4500 QTrap mass spectrometer, and two BEH HELIC analytical columns as recommended by Hopmans et al. (2016). We integrated peak areas from raw data with Sciex Analyst 1.7.2 and calculated the fractional abundances of individual isomers relative to their primary structure. A more detailed description of the brGDGTs extraction is available in the Supplementary Material.

We studied temporal changes in the sediment brGDGTs composition with established indices. We assessed temperature sensitivity with the indices MBT'_{5me} and MBT'_{6me} (Eq. (2) and Eq. (3)) (De Jonge et al., 2014), quantifying the degree of methylation. We evaluated changes in isomerization and cyclization with indices IBT, IR_{6me} and DC' (Eq. (4), Eq. (5) and Eq. (6)) (De Jonge et al., 2014; Ding et al., 2015; Dang et al., 2016; Damsté et al., 2009). We studied past changes in dissolved oxygen (DO) availability in the lake using the shifts in fractional abundances of isomers Ia, IIa and IIIa (Yao et al., 2020; Raberg et al., 2021; Wu et al., 2021; Ajallooeian et al., 2024).

To assess the potential primary source of brGDGTs, we compared the composition and the calculated Tippakuru sediment indices to those of modern lake biofilm and soil samples from Lake Annan Juomusjärvi catchment area (69°15′14’’N 27°24′21’’E) in northern Finland (Otiniano et al., 2024) by evaluating their similarity with K-means clustering using the packages *cluster* and *factoextra* in R version 4.3.3 (Kassambara and Mundt, 2020; Maechler, 2018). The comparison between the modern material from the Lake Annan Juomusjärvi locality and Lake Tippakuru is possible under the assumption that the similar local geology and Holocene environmental history resulted in comparable soil ecosystems. Additionally, we applied the machine learning algorithm BIGMaC (Branched and iso GDGT Machine learning Clark et al., 2001) to corroborate the potential source material of the sediment brGDGTs implied by the comparison with modern material.

$$MBTM_B^T = \frac{Ia + Ib + Ic}{Ia + Ib + Ic + IIa + IIb + IIc + IIIa} \qquad \text{Eq.2}$$

$$MBTM_B^T = \frac{Ia + Ib + Ic}{Ia + Ib + Ic + IIa' + IIb' + IIc' + IIIa'} \qquad \text{Eq.3}$$

$$IBT = -\log \frac{IIa' + IIIa'}{IIa + IIIa} \qquad \text{Eq.4}$$

$$IR_{6Me} = \frac{IIa' + IIb' + IIc' + IIIa' + IIIb' + IIIc'}{IIa' + IIb' + IIc' + IIIa' + IIIb' + IIIc' + IIa + IIb + IIc + IIIa + IIIb + IIIc} \qquad \text{Eq.5}$$

$$DC' = \frac{Ib + IIb + IIb'}{Ia + IIa + IIa' + Ib + IIb + IIb'} \qquad \text{Eq.6}$$

2.6. Climate reconstruction methods

2.6.1. Pollen

We prepared a pollen-based paleoclimate reconstruction using an ensemble of six pollen–T_{jul} calibration models. This ensemble has earlier been employed with two other fossil sequences recovered from the vicinity of Tippakuru, including the last interglacial sequence from Sokli (Salonen et al., 2018) and the Holocene sequence from Lake Kuutsjärvi

(Salonen et al., 2024). Further discussion on the calibration data, models, and validation of calibration models are found in Salonen et al. (2018, 2019). The calibration models used include three classical, unimodal transfer functions: the weighted averaging (WA; Birks et al., 1990), weighted averaging-partial least squares (WA-PLS; ter Braak and Juggins, 1993), and maximum likelihood regression curves (MLRC; Birks et al., 1990). We also used the modern analogue technique (MAT; Overpeck et al., 1985) as well as two machine-learning (ML) methods based on ensemble models of regression trees, the random forest (RF; Breiman, 2001) and the boosted regression tree (BRT; De'ath, 2007). The reconstruction errors of the models, estimated as the root-mean-square error of prediction in ten-fold cross-validation, range from 1.12 to 2.05 °C (Salonen et al., 2018). The calibration models were prepared in R using the libraries *gbm* (Ridgeway, 2020), *randomForest* (Liaw and Wiener, 2002), and *rioja* (Juggins, 2024).

In the pollen-based T_{jul} reconstruction, in addition to the new Tippakuru data we also included pollen data from the Holocene sequences from the nearby Lakes Loitsana (Salonen et al., 2013) and Kuutsjärvi (Salonen et al., 2024). With the six calibration models applied on each of the three sequences, this produced an 18-member ensemble T_{jul} reconstruction. To calculate a synthesis curve for the ensemble, we first interpolated all 18 reconstructions at 50-year time step, to equalize the impact of the reconstructions on the synthesis curve regardless of the sampling resolution of the underlying pollen dataset (Salonen et al., 2025). We then calculated the synthesis curve as the median of the 18 interpolated reconstructions, with multi-centennial features summarized as a five-point mean of the median curve (i.e., spanning 250 yr). The 95 % error margins for the synthesis curve were estimated by calculating the median 1000 times from bootstrap samples of the 18 ensemble members and then calculating the 2.5th and 97.5th percentiles. Finally, the synthesis reconstruction was expressed as anomalies vs. preindustrial (PI) by subtracting the mean of the synthesis curve over 250–50 cal a BP, representing the youngest five-point mean not overlapping with the industrial period (defined to start at 1900 CE).

2.6.2. Plant macrofossils

We performed plant macrofossil-based climate reconstructions using two probability-based approaches, CRACLE (Harbert and Baryiames, 2020) and CREST (Chevalier, 2022), implemented in R packages *cRacle* (version 1.1.1) and *crestr* (version 1.3.1). These approaches calculate the most likely climatic value of each given plant assemblage based on the normal (pCRACLE, CREST) and non-normal (nCRACLE) distributions of probability density functions representing modern climate-species relationships. For the modern calibration, we used mean July air temperatures from the CRU CL v.2.0 modern climate dataset (New et al., 2002) and modern plant observations downloaded from GBIF database (GBIF.org, 2024) (Fig. S3). The GBIF database was accessed using the R package *rgbif* version 3.7.7 (Chamberlain and Boettiger, 2017).

For plant macrofossil-based reconstructions, we used a subset of the modern taxon occurrence data, defined as the part of Eurasia where the Gorczyński Continentality Index (CI) is between 20 and 40, thus representing the modern-day continentality regime of Lake Tippakuru (CI = 32). We repeated the reconstruction for 50 iterations and each time used random 1500 modern plant observation data points (Fig. S3). For further discussion on the rationale of using the CI to select the calibration region, see Trasune et al. (2024).

2.6.3. brGDGTs

To reconstruct the Holocene months above freezing, we chose the region-specific high-latitude lacustrine brGDGT-temperature transfer function introduced by Otiniano et al. (2024). The transfer function was previously applied to Lake Annan Juomusjärvi in northeastern Finland (69°15′14"N 27°24′22"E), which has similar ecosystem characteristics to Lake Tippakuru (Table S2). The calibration data set comprises 117 modern samples from high-latitude lakes (57.2°N to 72.6°N and 14.6°W to 161.1°W; Martínez-Sosa et al., 2021; Raberg et al., 2021; Otiniano et al., 2023), and of T_{MAF} values calculated from ERA5 2-m air temperature reanalysis data (Hersbach et al., 2020) for the months of May to September (Otiniano et al., 2024). The transfer function is a multilinear step-backward regression ($\mathrm{ML_{fa}}$) that includes all fractions with a high correlation with T_{MAF} (Eq. (7)). We also compared the reconstruction against alternative published brGDGTs transfer functions and machine learning algorithms (Martínez-Sosa et al., 2021; Zhao et al., 2021; Bauersachs et al., 2024; Zhu et al., 2025).

$$T_{MAF} = 17 + 11.4 \times IIa - 17.4 \times IIIa - 15.9 \times IIa' - 124.4 \times IIIb \qquad \text{Eq.7}$$

2.7. Analysis of significant trends

We used generalized additive models (GAMs) to describe temporal trends and identify periods of change in brGDGTs isomer fractional abundances, brGDGT indices, and temperature reconstructions. The GAMs were fitted with the Restricted Maximum Likelihood method (REML) with smoothening (*sp*) and dimensionality (*k*) parameters suitable for each individual data resolution (Table S2), and a constant epsilon distance for all cases ($eps = 10^{-7}$) on *R* with the package *mgcv* (Wood, 2017). We identified the amount and timing for periods of statistically significant change in the time series as the first derivatives of the fitted splines in the GAMs, and the rate of change as the regression coefficient between points of significant change (Simpson, 2018).

3. Results

3.1. Age-depth model

The Lake Tippakuru age-depth model is based on 34 radiocarbon dates. It spans from 10.58 cal ka BP to the present, with the deepest 7 cm of the core obtained by extrapolation (Fig. 2; Table S1). The chronology curve consists of four linear trends with an average uncertainty of 185 yr and an alternating pattern of high and low sedimentation rates.

3.2. Vegetation development

3.2.1. Organic matter and plant macrofossil record

The plant macrofossil record, which spans from 10.5 cal ka BP to present, includes in total 17 taxa of trees, shrubs, and grasses, and other remains (Fig. 3). For the records of other organisms and charcoal particles observed during this analysis, see supplementary material (Figs. S1 and S2).

Until ca. 10 cal ka BP, sediments are highly minerogenic (≥100 sand grains/ml), while the organic matter content gradually increases. The tree-type *Betula* (incl. *B. pendula* and *B. pubescens*) is the first taxon with

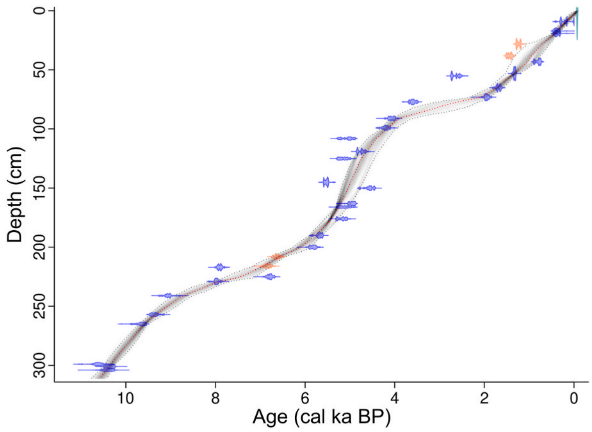

Fig. 2. Lake Tippakuru age-depth model with the calibrated ^{14}C dates (blue – plant remains; orange – bulk sediments) and the mean age estimates of the model (red curve) with 95 % confidence intervals (grey ribbon).

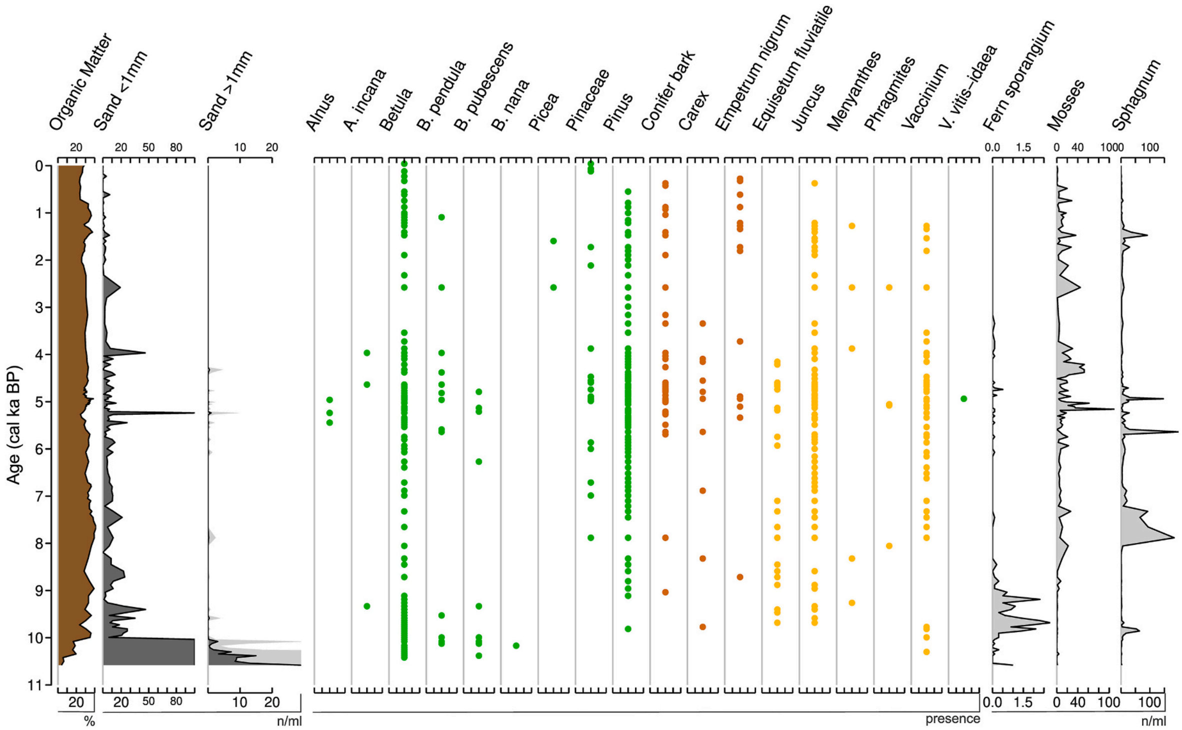

Fig. 3. Lake Tippakuru diagram of organic matter content (%), sand (n/ml), and identified plant macroscopic remains (presence or n/ml).

consistent presence alongside a single remain of *Betula nana* at 10.2 cal ka BP, and the shrub/dwarf shrub *Vaccinium*. By 10 cal ka BP, organic matter percentages reach 40 %, and sand grain concentrations drop rapidly as fern sporangia peak. The identified diversity of plant taxa increases with the appearance of *Alnus, Pinus*, and the wetland plants *Carex*, *Equisetum*, *Juncus*, and *Menyanthes*. Starting from ca. 8 cal ka BP, sediments are rich in plant macrofossils with near-constant presence of *Betula*, *Pinus*, *Vaccinium*, and *Juncus*. A strong *Sphagnum* moss peak appears from ca. 7.9 to 7.3 cal ka BP. Between ca. 6 and 4 cal ka BP *Alnus* (incl. *A. incana*) is present, with increased fern sporangia and moss concentrations. Sand grain (<1 mm) concentrations fluctuate over the mid and late Holocene, with one sample at 5.2 cal ka BP having above background (≥100 grains/ml) presence, corresponding to a slight drop in organic matter content. At 3.9 cal ka BP *Menyanthes* reappears, fern sporangia disappear completely, and moss concentration increases slightly. At 2.6 cal ka BP *Picea* needle fragments appear. At ca. 1.2 cal ka

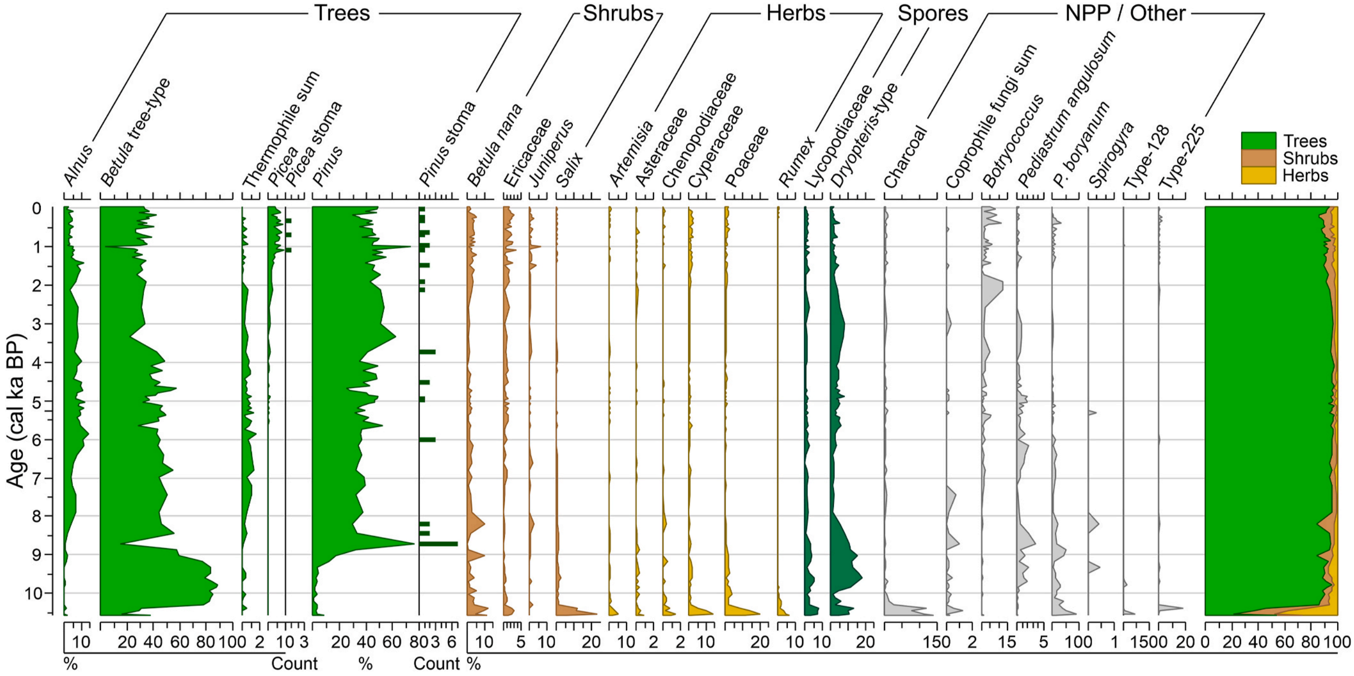

Fig. 4. Lake Tippakuru pollen diagram, including spores, non-pollen palynomorphs (NPPs) and conifer stomata. Values are shown as percentages for pollen, spores, and NPPs, and as absolute counts for stomata. Selected taxa are shown; for full data see Supplementary Data.

BP macrofossil diversity decreases.

3.2.2. Pollen record

Pollen records (Fig. 4) starts at 10.6 cal ka BP and indicate low (20 %) tree pollen, but high shrub (30 %) and herb (50 %) values until ca. 10.3 cal ka BP, after which tree pollen rises with high *Betula* pollen values of 80–90 % and *Pinus* at ~5 %. At ca 8.7 cal ka BP *Pinus* shortly peaks and reaches 75 % as *Betula* drops to 15 %. At around 8.2 cal ka BP, total tree presence decreases by 10 %, and is replaced by shrubs, seen as a peak in *Betula nana* and *Juniperus*. Simultaneously, we note a presence of *Spirogyra* algae, a near or complete disappearance of many herbs (*Artemisia*, Asteraceae, Cyperaceae, and Poaceae), and a decrease in spores (Lycopodiaceae, *Dryopteris*-type). By 7.9 cal ka BP, both *Betula* and *Pinus* pollen percentages stabilize with values from 40 % to 50 % (*Betula*) and from 30 to 40 % (*Pinus*), while *Betula nana* and spores stay at <5 %. Starting from ca. 2.5 cal ka BP, total tree pollen decreases from ~95 % to 85–90 % as *Betula nana*, *Juniperus,* Ericaceae, Cyperaceae, and Poaceae percentages increase. At ca. 1 cal ka BP, *Pinus* again briefly peaks and reaches 75 %, and is accompanied by an increase in *Juniperus*, while *Betula* decreases to around 5 %.

3.3. Sediment brGDGTs composition and potential origin

The sediment record is dominated by uncyclized brGDGTs, with Ia, IIa, IIIa, and IIa’ having each a Holocene average fractional abundance of ≥5 %, and their sum accounting for 88 ± 3 % of the total. The Tippakuru sediments are compositionally similar to the biofilm of Lake Annan Juomusjärvi rather than to soil samples from its catchment (Fig. S5), suggesting a lake source. Furthermore, the index CBT’, strongly correlated to soil pH (Damsté et al., 2009), is higher in the soils samples than in the biofilm and sediment samples (Fig. S5), also implying a lake source. Likewise, the indices DC’ (Damsté et al., 2009) and IBT (Ding et al., 2015), which measure the degree of cyclization related to membrane fluidity, are lower in the soil samples (DC’ = 0.01 ± 0.01, IBT = −0.9 ± 0.3) than in biofilm (DC’ = 0.05 ± 0.008, IBT = −0.5 ± 0.08) and sediment samples (DC’ = 0.08 ± 0.02, IBT = −0.5 ± 0.1) (Fig. S5). In addition, the BIGMaC algorithm (Martínez-Sosa et al., 2023) identifies most of the record as lake-type GDGTs (Fig. 5). Therefore, we assume the majority of brGDGTs in Tippakuru lake sediments are likely of lacustrine origin throughout the Holocene and reflect T_{MAF}.

The sediment record shows temporal changes in methylation isomerization and composition. The beginning of the record at ca. 10 cal ka BP has lower MBT’$_{6\mathrm{Me}}$ values that increase gradually until ca. 6 cal ka BP (from 0.65 to 0.75; Fig. 5D), and higher IBT values that decrease simultaneously (−0.4 to −0.6; Fig. 5C), indicating higher presence of penta- and hexamethylated isomers at the C6′ position. Between ca. 6 and 4 cal ka BP, there are shifts in methylation and isomerization, as suggested by the drop in MBT’$_{6\mathrm{Me}}$ and MBT’$_{5\mathrm{Me}}$ (0.8–0.7 and 0.4 to 0.3 respectively), and the rise in IBT (−0.7 to −0.5; Fig. 5). The main change in brGDGT distribution after ca. 6 cal ka BP is the increase in IIIa fractional abundance (Fig. 5B), which continues until the present from 22 % to 30 %, and the decrease in IIa fractional abundance after ca. 3 cal ka BP from 34 % to 30 %.

3.4. Temperature reconstructions

Temperature reconstructions from Tippakuru (Fig. 6) start with anomalies of +0.5 °C for plant macrofossils (Fig. 6A), +0.4 °C for brGDGTs (Fig. 6B), and −1.8 °C for the median pollen-T_{jul} across all methods (Fig. 6D, solid line), followed by a warming starting ca. 10.5 cal ka BP with rates of +0.18 °C/kyr, +0.2 °C/kyr and +0.7 °C/kyr until 7.2 cal ka BP, 6.8 cal ka BP and 5.5 cal ka BP, respectively. The reconstructions reach the maximum temperature (anomalies between +1 °C and +1.8 °C) around the mid Holocene (6.8 cal ka BP for plant macrofossils, 5.8 cal ka BP for brGDGTs, and 5.5 cal ka BP for pollen. The reconstructions from plant macrofossils and pollen suggest a period of stable warm temperatures until ca. 2.7 cal ka BP and 3.4 cal ka BP, respectively, after which there is a cooling with a rate of −0.4 °C/ka until present. In contrast, brGDGTs show an abrupt cooling of 0.9 °C after the peak in temperatures ca. 5.8 cal ka BP.

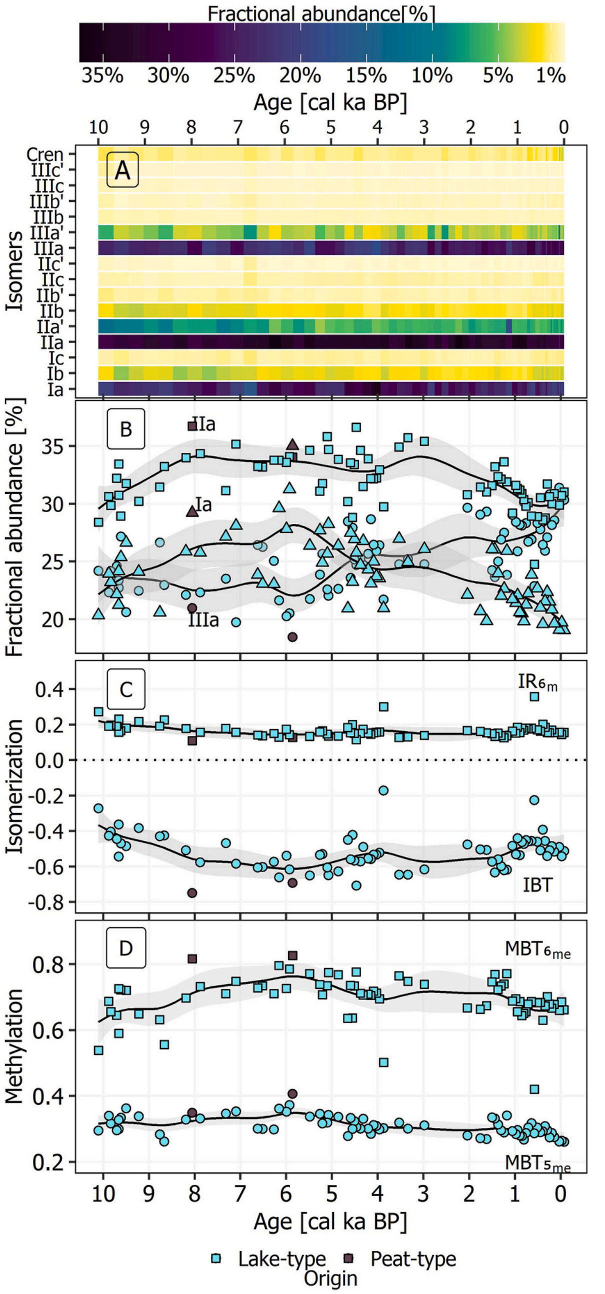

Fig. 5. Holocene sediment GDGT distribution and common indices for Tippakuru. **A.** brGDGT and crenarchaeol fractional abundances. **B.** Time-series plot of Ia (triangle), IIa (square), and IIIa (circle) fractional abundance. **C.** Isomerization indices IBT and IR$_{6\mathrm{M}}$. **D.** Methylation indices MBT$_{5\mathrm{Me}}$ and MBT$_{6\mathrm{Me}}$. The origin of GDGTs calculated with the BIGMaC algorithm (Martínez-Sosa et al., 2023) is indicated with the colors: light blue for lake-type and dark purple for peat-type. The indices and uncyclized isomers series are smoothed with GAMs with parameters $k = 30$ and $sp = 0.1$.

A pollen-based reconstruction also incorporating the pollen sequences from the nearby lakes Loitsana and Kuutsjärvi (Fig. 7) largely repeats features of the Tippakuru-only reconstruction. Major between-site differences are seen in the timing of the possible HTM, with Loitsana indicating an early warm peak at approximately 8–7 cal ka BP, while Kuutsjärvi record suggests the warmest period starting at 6–4.8 cal

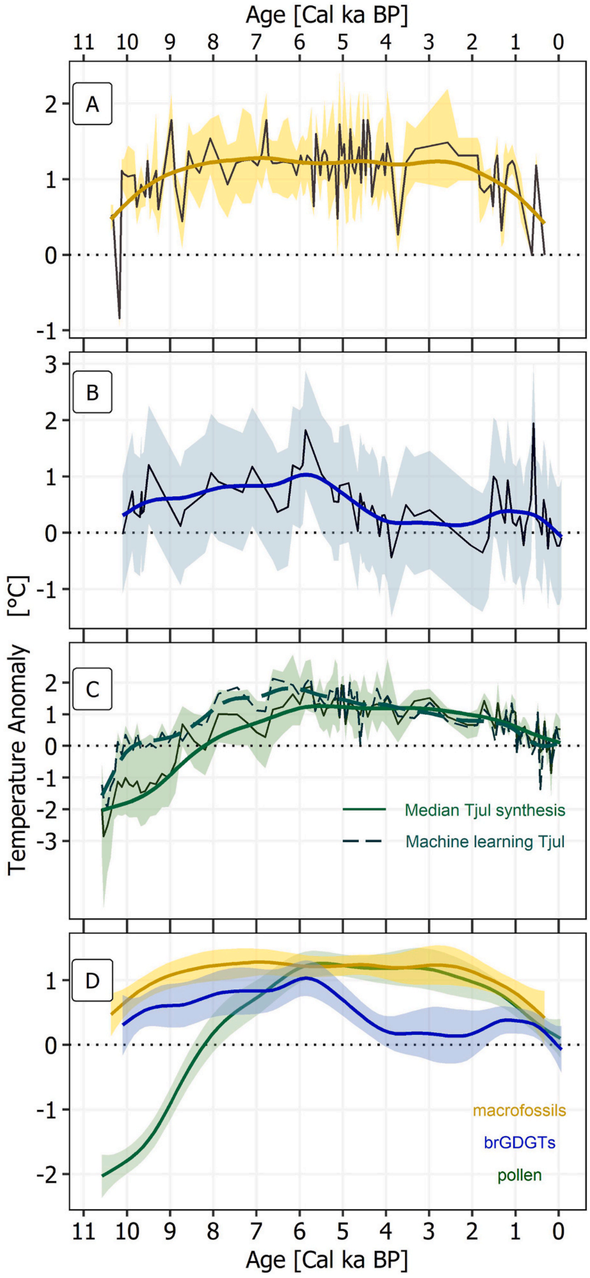

Fig. 6. T_{jul} and T_{MAF} anomalies of Lake Tippakuru. **A:** plant macrofossil-based T_{jul} anomalies (vs. the youngest sample at 324 cal a BP); **B:** brGDGT-based T_{MAF} anomalies vs. preindustrial (PI); **C:** pollen-based T_{jul} anomalies vs. PI; **D:** comparison of the reconstructed temperature anomalies between all three proxies. The temperature reconstructions are fitted with GAMs depending on the data resolution of each proxy (using *k* values of 45 for plant macrofossils, 30 for brGDGTs and 40 for pollen, and *sp* of 0.1 for all proxies).

ka BP (Salonen et al., 2024). Lake Tippakuru record, in turn, indicates a longer warm period spanning from 8 to 4 cal ka BP, which aligns with the pollen-based synthesis curve. A clear 8.2 ka event is seen in the three-site T_{jul} synthesis curve, largely driven by the Kuutsjärvi record, but also seen in Lake Tippakuru as a a sharp fall in tree pollen (Fig. 4). While the 8.2 ka event is clearly visible as a fall in reconstructed T_{jul}, we note that Salonen et al. (2024) express reservations about whether the distinct opening of tree cover, while closely aligning with the negative excursion in ice core δ^{18}O values in Greenland (Rasmussen et al., 2007), can be specifically attributed to a summer temperature reduction as opposed to a change in some other climate variable.

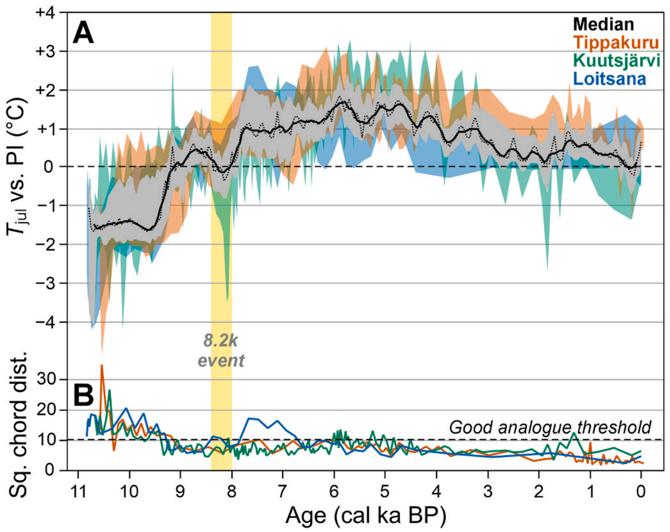

Fig. 7. Pollen-based mean July temperature (T_{jul}) synthesis reconstruction incorporating three pollen sites (Tippakuru, Kuutsjärvi and Loitsana). **A:** T_{jul} synthesis curve, incorporating 18 individual reconstructions using six pollen-climate calibration models on each of the three pollen sequences. The *dotted black line* represents the median of the 18-member ensemble and the *thick black line* a five-point mean of the ensemble median. The *grey band* represents the 95 % error margins of the ensemble median, estimated as the 2.5th and 97.5th percentiles of the median when calculated from 1000 bootstrap samples of the ensemble members. The *colored bands* represent the 95 % error margins of the site-specific reconstructions, calculated from bootstrap samples of the reconstructions from the ensemble of six calibration models. Reconstructions are expressed as deviations from the preindustrial (PI) mean (*dashed line*), defined as the average of the ensemble median over 250–50 cal a BP. **B:** the modern analogue quality for each fossil pollen sample, calculated as squared-chord distance to the best-matching modern pollen sample in the calibration data-set. The *dashed line* indicates the threshold value for a good modern analogue (10.32), calculated as the 5th percentile of the between-sample squared-chord distances in the calibration data. The *yellow bar* indicates the timing of the 8.2 ka abrupt climate event (8.4–8.0 cal ka BP) in Greenland ice core data.

4. Discussion

In this chapter, we discuss the differences between reconstructed Holocene climate trends across our proxies. We divide the discussion into three subsections, each describing a distinct climatic period: early Holocene (EH), mid-Holocene (MH), and late Holocene (LH). We acknowledge that our proxies represent different moments of the warm season, however, for our research purpose we assume the temperature anomalies follow the same long-term trends of the Holocene.

4.1. Discrepancies in early Holocene warming between proxies

Our multi-proxy reconstructions indicate different climate trends during the onset of the Holocene: the pollen synthesis curve suggests colder than present warm-season temperatures while plant macrofossils and brGDGTs show already warm conditions in the EH. The rate of this warming ranges between +0.2 °C/kyr (plant macrofossils, brGDGTs) and +1.3 °C/kyr (pollen synthesis) between the period 10.6 cal ka BP and 5.5 cal ka BP (Table 1). Similar uncertainties of EH warming trends are observed in other localities across Europe (Mateo-Beneito et al., 2024; Shala et al., 2017; Väliranta et al., 2015) and can even be seen between individual pollen records (Bjune et al., 2004; Salonen et al., 2019). Several factors could be linked to these discrepancies.

Although both brGDGTs and plant macrofossils indicate an overall warm growing season at the onset of the Holocene, plant macrofossil-T_{jul} could potentially be biased by false absences of taxa in sediments (Birks and Birks, 2000). It is typically assumed that plants found in the record

Table 1

Significant inflection points and rate of change in Lake Tippakuru temperature reconstruction anomalies across proxies calculated with GAMs. Note the gap in the brGDGTs record between 3.3 cal ka BP and 1.2 cal ka BP (Fig. 5), hindering the calculation of the rate of change for this period. Table S3 expands on the data resolution, GAM parameters, and significant inflection points and rates of change for the pollen-based reconstructions from Lakes Kuutsjärvi, Loitsana and regional synthesis reconstructions, and brGDGTs-based Annan Juomusjärvi.

Proxy	Significant inflection points			Trends		
	Total changes	Age [ka]	Temp. Anomaly [°C]	Start [ka]	End [ka]	Rate of change [°C/kyr]
brGDGTs	7	7.2	0.9	10.1	7.2	0.2
		6.9	0.9	6.9	5.8	0.2
		5.8	1.1	5.8	3.3	−0.5
		3.6	0.2	1.2	Present	−0.4
		3.3	0.2			
		2.4	0.2			
		1.2	0.4			
Plant macr.	5	6.8	1.3	10.4	6.8	0.2
		5.5	1.2	6.8	5.5	−0.2
		4.6	1.2	5.5	4.6	0.2
		3.7	1.2	4.6	3.7	−0.2
		2.7	1.2	2.7	Present	−0.4
Pollen	3	5.5	1.2	10.6	5.5	0.7
		4.1	1.2	5.5	4.1	0.0
		3.4	1.2	3.4	Present	−0.4

represent a strongly established community in the catchment: a true presence of a population. Regardless of whether it is objectively true, our reconstruction algorithms assume these populations are growing in their most optimal climatic conditions. Thus, our calculations might possibly lead to overestimation or underestimation of the plant macrofossil-T_{jul}. However, an independent variant of the climate indicator plant species method, based on the northern distribution limits of indicator plants (Isarin and Bohncke, 1999; Väliranta et al., 2015), which reduces this issue by interpreting the climatic value from the median of the minimum T_{jul} of the most warmth-requiring taxa in the vegetation, provide similar warm EH absolute temperatures to ours (Fig. S4) for the nearby Lake Kuutsjärvi (Salonen et al., 2024). Therefore, despite different methodologies, plant macrofossils are in an agreement with the warm EH scenario in Northern Europe (e.g., Väliranta et al., 2015; Luoto et al., 2014; Cremer et al., 2004). Moreover, our brGDGT T_{MAF} reconstructions also suggest a warm EH at Lake Tippakuru during the whole warm season (Fig. 6B and S5). We, however, see major discrepancies between our reconstructed T_{MAF} values and those from Lake Annan Juomusjärvi, also located in northern Finland, ca. 190 km north from Lake Tippakuru (Otiniano et al., 2024).

Interestingly, the T_{MAF} reconstruction from Lake Annan Juomusjärvi (Otiniano et al., 2024) agrees well with pollen-based T_{jul} reconstructions from Loitsana and Tippakuru using the MAT, WA, and WA-PLS calibration models (Fig. 7 and S8), implying that cold EH conditions were widespread in Northern Finland. A possible reason for the EH temperature disparity between brGDGT-based reconstructions from Lake Tippakuru and Lake Annan Juomusjärvi might be due to differences in microbial communities determining the brGDGTs composition. Environmental factors including ice cover seasonality (Loomis et al., 2014; Cao et al., 2020; Zhu et al., 2021), in-situ versus exogenic lipid source (Weber et al., 2015; Martínez-Sosa et al., 2021; Raberg et al., 2022; Wang et al., 2023), salinity (Liang et al., 2024; Zhu et al., 2025), oxygen depletion (Yao et al., 2020; Wu et al., 2021; Ajallooeian et al., 2024; Raberg et al., 2025), and lake depth (Stefanescu et al., 2021) are known to influence lacustrine brGDGT composition. Despite similarities between both lakes with respect to depth, water chemistry and seasonality (Table S2), Lake Annan Juomusjärvi has a higher isomerization (IR_{6ME} ~0.4; Otiniano et al., 2024) than Lake Tippakuru (IR_{6ME} ~0.2; Fig. S7) at ca. 10 cal ka BP. A higher isomerization can result from non-thermal factors and bias MBT_{5Me}-based temperature reconstructions (Wang et al., 2024). In middle to high-latitude lakes, IR_{6ME} value ≥ 0.4 suggests a weaker temperature response of brGDGTs than values below this IR_{6ME} cutoff (Novak et al., 2025). While only three samples from the Lake Annan Juomusjärvi record exceed the suggested cutoff value at the beginning of the EH, many samples plot close to it (Fig. S7), and at least some of the reconstructed EH temperatures should be considered with caution.

An alternative explanation for the EH T_{MAF} discrepancy between both brGDGTs records is a thermal gradient from the northern coastal zone to inland, where EH T_{jul} simulations suggest temperature differences of ~2 °C (Schenk and Wohlfarth, 2019; Kuang et al., 2021; Salonen et al., 2024), as a result of the cold air brought from the Nordic Seas to Fennoscandia by westerly to northerly winds. Pollen records from Northeast Norway and Northwest Russia (Seppä et al., 2002, 2008) and brGDGTs records from Kola peninsula (Holtzman et al., 2025), also suggest a cold but rapidly warming EH, while numerous other temperature reconstructions from northern Fennoscandia suggest a warm EH (Sjögren, 2021). None, however, are in close proximity to Lake Annan Juomusjärvi, hindering the comparison. To further investigate the potential cause of the inconsistency in T_{MAF} reconstructions between the two sites, a study of bacterial communities and the seasonal production of lacustrine brGDGTs in both lakes is recommended to better understand the ecological drivers of sediment brGDGT composition. Furthermore, more brGDGT-based temperature reconstructions from northern Europe are needed to clarify EH drivers of brGDGT assemblages in this region.

If warm conditions prevailed during the EH in our study area, then why do pollen fail to show similar trends as brGDGTs and plant macrofossils? It is possible that a lag in vegetation response rates due to the rapidly changing climate (Webb, 1986; Birks et al., 2011; Väliranta et al., 2015) could be a major factor for colder reconstructed EH pollen-based T_{jul}. The increased dissimilarity index we see during EH (Fig. 7B), might indicate such disequilibrium conditions, where vegetation has not fully established in the relatively recently deglaciated Northern Finland. Additionally, long-distance pollen transport can affect the interpreted vegetation, particularly in treeless and tree-line areas (Birks and Birks, 2000), such as postglacial Värriö region, as seen in the appearance of new tree taxa in the EH vegetation records (Figs. 3 and 4; Salonen et al., 2024; Shala et al., 2017). Under the assumption that the winds during the warm season mainly follow westerly to northerly patterns rather than the modern-day southwesterly direction (Salonen et al., 2024), this, in theory, could affect the presence and concentration of, for example, thermophile taxa in pollen assemblages leading to underestimation of pollen-T_{jul} values.

It is also noteworthy, however, that our pollen-T_{jul} reconstruction ensemble of the EH shows considerable spread between the calibration methods used (Fig. 6D and S8), and hence, the EH offset compared to plant macrofossils and brGDGTs is not a robust feature of the pollen-based ensemble reconstruction. The median synthesis curve, which considers all methods, has an anomaly of −2 °C vs. PI at ca. 10.5 cal ka BP, however, the T_{jul} generated with the methodologically distinct ML-based algorithms (RF and BRT) has an anomaly of −0.8 °C (Fig. 6). Considering that both brGDGTs and plant macrofossil records begin hundreds of years after pollen, the ML-based reconstructions show similar temperature estimates as local proxies after ca. 10 cal ka BP. This between-method spread in the pollen-based reconstructions may be explained by the distinct ways the individual calibration approaches deal with the EH pollen samples which generally lack good modern analogues (Fig. 7B). Notably, the EH pollen samples from Tippakuru for 10.3–9.3 cal ka BP have *Betula* values averaging at 85 % which greatly exceeds the *Betula* values seen in the modern calibration data, where only 2 % of samples record *Betula* at over 60 % and the maximum reached is 74 %. The different calibration models deal with these non-analogue taxon percentages in starkly different manners. The commonly used unimodal methods WA and WA-PLS emphasize the *Betula* dominance in the paleoclimate reconstructions and give proportionally increasing weight to the modern modelled T_{jul} optimum of *Betula*, i.e., when (fossil) *Betula* values exceed that of modern *Betula*, WA and WA-PLS calculate T_{jul} by extrapolation.

In contrast, our ML methods (RF and BRT), which are based on regression-tree models, implicitly truncate the range of the taxon variation. Any (fossil) *Betula* value which exceeds the modern *Betula*, is regarded as equal to the highest *Betula* value within modern calibration data. This limits the impact of the non-analogue high values on the reconstruction. Moreover, regression-tree models are selective in using predictor variables (De'ath and Fabricius, 2000) (here, pollen taxa), and the models may heavily employ comparatively rare pollen types if they have been proven to be useful predictors during the calibration model building process, while potentially ignoring common but less climatically informative pollen types (Salonen et al., 2019). For example, in our BRT model for T_{jul}, *Betula*, despite its prolific numbers in the modern calibration samples, has a mere 3.8 % contribution to the model (Salonen et al., 2019). Together, these characteristics of regression-tree models may make the ML-based reconstructions less sensitive to the exceptional *Betula* percentages in the fossil samples. If we consider only the mean of the two ML reconstructions (−0.8 °C, Fig. 6C), the discrepancy between pollen, and plant macrofossils (+0.3 °C, Fig. 6A) and brGDGTs (+0.5 °C, Fig. 6B) would be smaller, and uniformly favour a warm EH scenario. More generally, our observation implies that some of the northern European early-postglacial temperature reconstruction disagreements observed between pollen and other proxies including chironomids (Salonen et al., 2019) and aquatic plant macrofossils (Väliranta et al., 2015), could be addressed by supplementing the classical methods commonly used in the region (especially WA-PLS) with alternative proxy calibration approaches.

Another notable difference between local and regional proxies is that the plant macrofossil and brGDGT records are of lower resolution than the pollen records. This, in turn, leads to insufficient data to reconstruct short-term climatic events such as the 8.2 ka cooling – an event which briefly interrupted general warming trends of EH (Alley and Agustsdottir, 2005; Alley et al., 1997). Although each of our records indicates some environmental disturbances possibly related to the 8.2 ka event, including changes in vegetation, origin of brGDGTs, and a possible peak in charcoal particle count (Figs. 3–5 and S2), an identifiable change in temperature is evident only in pollen-based reconstructions (Fig. 7). To compare the 8.2 ka event in our pollen-based T_{jul} reconstruction with those from plant macrofossils and brGDGTs, a higher proxy-data resolution would be needed.

In summary, plant macrofossils, brGDGTs, as well as a subset of the pollen-based ensemble reconstruction support the evidence of warm EH growing-season conditions in Northern Europe (e.g., Väliranta et al., 2015; Luoto et al., 2014; Cremer et al., 2004) with temperatures up to ~1 °C warmer than present. However, we observe discrepancies between proxies, the individual members of pollen-based ensemble reconstruction, and individual brGDGT records from the same region. This underlines the importance of preparing synthesis reconstructions incorporating multiple proxy sites, a range of proxy types, and an ensemble of quantitative reconstruction algorithms. As shown by our results, such ensemble can help control for the biases that may show up with individual sites, proxies or numerical methods, and help reach an estimate of the most likely regional climate history.

4.2. The warm-season temperature trends of the mid-Holocene

Around 6 cal ka BP, plant macrofossil T_{jul} and pollen-based T_{jul} reconstructions fully converge and indicate continuous warm MH conditions with a positive anomaly between ~1.3 °C (plant macrofossils; Fig. 6A–Table 1) and 1.5 °C (pollen; Fig. 7, Table 1), while brGDGTs show a drop in T_{MAF} by ~1 °C (Fig. 6B–Table 1). The data, hence, suggest a possible turning point of local and regional environmental conditions. However, we identify major uncertainties within our reconstructions: the timing of the convergence between vegetation proxies during the MH, against a decrease in brGDGTs-T_{MAF} values.

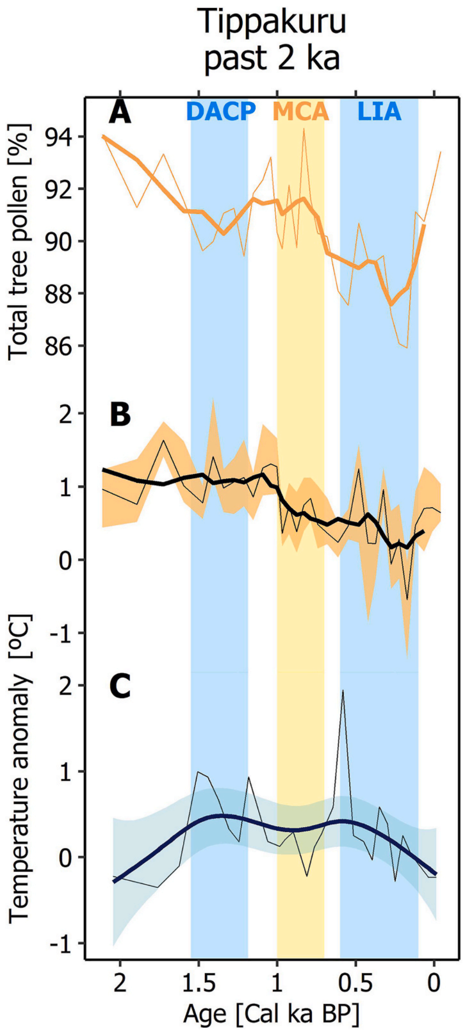

Fig. 8. Tree pollen and temperature changes in the late Holocene. **A:** Total tree pollen; **B:** Pollen-based T_{jul} anomalies vs. PI; **C:** brGDGT-based T_{MAF} anomalies vs. PI; Abbreviations: DACP – Dark Ages Cold Period; MCA – Medieval Climate Anomaly; LIA – Little Ice Age.

Our vegetation-based reconstructions agree with reports of temperature anomalies between 1 and 3 °C during the warmest phase of the Holocene (e.g., Bjune et al., 2004; Kaufman et al., 2020; Renssen et al., 2012; Salonen et al., 2019; Seppä et al., 2009; Wanner et al., 2015). The exact timing of when the T_{jul} reached its highest values in our Lake Tippakuru reconstructions and the pollen-based multi-site synthesis reconstruction (Figs. 6 and 7) is, however, not clear. We again note important differences between the classical and ML-based reconstruction algorithms for pollen. For example, pollen-based ensemble T_{jul} reconstructions of Lake Tippakuru reaches the T_{jul} reconstructed from plant macrofossils- (+1.2 °C) by 5.5 cal ka BP (Fig. 6, Table 1). A study by Väliranta et al. (2015) reports that by 7.5 cal ka BP plant macrofossil-inferred T_{jul} were up to 2 °C warmer than pollen-T_{jul} across multiple sites of Northern Europe, which is consistent with our pollen records (Fig. 6). However, both the ML-based algorithms (Fig. 6C) and the pollen-based synthesis curve (Fig. 7) indicate a positive T_{jul} anomaly of ~1 °C by ca. 8 cal ka BP. These observations reinforce that the paleoclimatic conditions inferred from pollen depend considerably on the methodological choices during the pollen–climate calibration, and that the range of plausible climate histories is best assessed using an ensemble reconstruction approach.

In contrast to vegetation-based proxies, the continuous warming trend of 0.2 °C/kyr seen in brGDGT T_{MAF} records abruptly ends at 5.8 cal ka BP (Fig. 6, Table 1), and is followed by an immediate cooling of −0.5 °C/kyr until present (Fig. 6). Moreover, Lake Annan Juomusjärvi T_{MAF} has a similar cooling trend (−0.1 °C/kyr, Table S3) between 6.2 and 4.6 cal ka BP, which is more pronounced in alternative MBT_{5Me} and machine learning reconstructions (Fig. S6). In both T_{MAF} records, the reconstructed cooling is driven by the increase in brGDGT IIIa: an important component of the T_{MAF} transfer function (Eq. (7)), and an abundant isomer in both sediment records. This isomer has a high correlation with cold temperatures (De Jonge et al., 2014; Russell et al., 2018; Ajallooeian et al., 2024) and is the most abundant isomer in high-latitude lacustrine brGDGTs (Zhao et al., 2023; Otiniano et al., 2023, 2024). The shifts in uncyclized brGDGTs, especially IIIa, are also associated with low DO levels or seasonal hypoxia (Yao et al., 2020; Wu et al., 2021; Ajallooeian et al., 2024; Raberg et al., 2025), implying a possible non-thermal cold bias in the reconstruction (Raberg et al., 2025). Both Lake Tippakuru and Lake Annan Juomusjärvi are oligotrophic, shallow, open systems where anoxia during the warm season is unlikely. Opposing shifts in isomers IIIa and Ia, similar to those seen in Lake Tippakuru (Fig. 5B) record, have been associated with deoxygenation (Raberg et al., 2021, 2025). However, the evidence is limited to a few study sites. Hence, we underscore the need to further study lake-specific environmental drivers and microbial communities impacting brGDGT assemblages at our study site. Moreover, we observe the same cooling pattern when testing other brGDGDT transfer functions less sensitive to changes in IIIa (Fig. S6), thus reducing the possibility of an artifact caused by IIIa alone. Furthermore, we see a similar decline in pollen-based T_{jul} in Lake Kuutsjärvi (at 5.4 cal ka BP, Table S3) (Salonen et al., 2024) together with increased modern analogue distances (Fig. 7B), and, to a lesser degree, a decline in pollen-based T_{jul} in Lake Loitsana (at 6.8 cal ka BP, Table S3) (Shala et al., 2017). Otiniano et al. (2024) linked T_{MAF} reconstructions of Lake Annan Juomusjärvi with the end of the warm season (May to September) related to the decrease in mean relative insolation starting at ca. 6 cal ka BP (Fig. S6) (Laskar et al., 2004). A similar behaviour is seen in Lake Tippakuru T_{MAF} (Fig. S6), which urges a detailed analysis of seasonal changes in lacustrine brGDGTs composition at both sites. The period in which the brGDGT producing bacteria are more active varies from site to site (Miller et al., 2018; Loomis et al., 2014; Qian et al., 2019). Without further proof and analysis of the seasonal ecosystem characteristics of Lake Tippakuru and Lake Annan Juomusjärvi, we can only speculate that overall changes in the end of the warm season could have affected brGDGT production during the end of the MAF season. In summary, the MH trends of warm season differ between the vegetation and brGDGT proxies. Our results suggest that brGDGT-based T_{MAF} might be sensitive to the shifts during the end of the warm season rather than the whole MAF, compared to vegetation proxies which traditionally represent the warmest point of the season. This observation reinforces the need for multi-proxy and multi-method comparisons, and a deeper understanding of brGDGT response to the variations within the MAF season.

4.3. *The (in)visible trends in the late Holocene climate*

Our records (Figs. 7 and 8) agree with the strong evidence of the orbitally driven warm-season cooling across terrestrial and marine records of northern high latitudes (e.g., Wanner et al., 2008; Eldevik et al., 2014), and show a temperature decrease rate of −0.4 °C/kyr during the late Holocene (Table 1). In addition to the long-term cooling trend during the LH, shorter multi-centennial environmental and climatic disturbances are also present in the Tippakuru pollen and brGDGT records (Fig. 8), broadly corresponding with the climatic anomalies of the Common Era (CE – last 2000 yr) known as the Dark Ages Cold Period (DACP; 400–765 CE or 1.5–1.2 cal ka BP) (Helama et al., 2017), the Medieval Climate Anomaly or the Medieval Warm Period (MCA: 950–1250 CE or 1–0.7 cal ka BP) (Mann et al., 2009), and the Little Ice Age (LIA; 1350–1850 CE or 600–100 cal a BP) (IPCC, 2007). Due to low data resolution, no distinct short-term variations can be identified in the plant macrofossil record and its T_{jul} reconstruction.

The distinct tree pollen variations at Tippakuru align with the DACP/MCA/LIA events (Fig. 8A) and likely indicate a downward movement of the tree line in the low mountains surrounding the lake. However, these events are not as reflected in pollen-based reconstructed T_{jul} (Fig. 8B). This is likely explained by the fact that these shifts in the tree pollen curve are largely driven by variations in (non-arboreal) *Betula nana* (Fig. 4). By contrast, the modern calibration data for pollen, which underpins the T_{jul} reconstruction, does not include *B. nana* separately but only includes an undifferentiated *Betula* column. Due to this, although *B. nana* has been identified separately for Lake Tippakuru, it is also pooled with the tree-type *Betula* for the pollen-based T_{jul} reconstruction. Hence, for the past 2 kyr, where *B. nana* is a major component of the total pollen variation, it is plausible the total tree pollen curve is more climatically informative than the T_{jul} reconstruction. The reconstructed brGDGT-based T_{MAF}, on the other hand, shows high instability with temperatures oscillating from −0.3 °C to +1.9 °C relative to PI (Fig. 8C). While we see some climatic variability, it is likely a reflection of a reconstruction noise caused by the high sensitivity of brGDGTs to different environmental changes (Martínez-Sosa et al., 2020). In general, the presence of LH warm-season short-term trends across the proxies are highly affected by the data resolution, characteristics of calibration dataset and proxy responses to non-climatic factors.

5. Conclusions

- There are clear inconsistencies in the rate and duration of the EH warming trends between the Lake Tippakuru reconstructions based on different climate proxies (pollen, plant macrofossils, brGDGTs). These discrepancies could stem from proxy-specific biases linked to accumulation and preservation of fossil material, non-climatic factors and their proxy-specificity,or methodological choices surrounding the reconstruction. For example, we see that pollen-based T_{jul} for the EH is highly dependent on the chosen reconstruction algorithm, highlighting the importance of evaluating multi-method reconstructions. Additionally, the differences between brGDGT-based reconstructions from Tippakuru and the previously published brGDGTs records from the northern Fennoscandian coastal region are yet to be fully explained.
- In the MH, the vegetation proxies strongly agree on stable and warm T_{jul} conditions around Lake Tippakuru. BrGDGTs, however, indicate a drop in T_{MAF} at ca. 5.8 cal ka BP, followed by continued colder warm-season temperatures until the present with some variations over time. We link the T_{MAF} decrease to shifts in abundance of brGDGT-IIIa due to its weight in the transfer function and its high correlation to cold temperatures. However, we acknowledge that further research on the uncertainties surrounding the proxy relationship to thermal and non-thermal environmental conditions is needed.
- All three proxies agree on a LH cooling trend of approximately −0.4 °C/kyr coinciding with a declining insolation in the high latitudes. Meanwhile, none of the proxies indicate short-term variations in warm-season temperatures, although the ability to detect such fluctuations could be hindered by proxy-specific drawbacks, including an insufficient data resolution in plant macrofossils, the loss of climate signal in the pollen-based reconstruction due to the taxonomic harmonization of the pollen data, and a likely response to non-climatic factors impacting brGDGTs.

Author contributions

Liva Trasune: conceptualization, data curation, formal analysis, investigation, validation, visualization, writing – original draft, writing – review & editing. **Lilia E. Orozco:** conceptualization, data curation, formal analysis, validation, visualization, writing – original draft, writing – review & editing. **J. Sakari Salonen:** conceptualization, data curation, formal analysis, investigation, validation, visualization, writing – review & editing. **Gerard A. Otiniano:** resources, formal analysis, writing – review & editing. **Trevor J. Porter:** resources, formal analysis, writing – review & editing. **Jan Weckström:** conceptualization, investigation, writing – review & editing. **Michael A. Phillips:** resources, formal analysis, writing – review & editing. **Frederik Schenk:** conceptualization, formal analysis, writing – review & editing. **Maija Heikkilä;:** conceptualization, writing – review & editing.

Declaration of competing interest

The authors declare that they have no known competing financial interests or personal relationships that could have appeared to influence the work reported in this paper.

Acknowledgements

This study was supported by the Research Council of Finland projects 331426 (JSS) and 334509 (MH). FS is funded by the Swedish Research Council for Sustainable Development (FORMAS 2020-01000; 2023-01631). TP is funded by the Natural Sciences and Engineering Research Council of Canada (RGPIN-2023-05448). We thank the staff of Värriö Research Station and Niina Kuosmanen for their help during the fieldwork, and Minna Väliranta for her help during the lab work.

Appendix A. Supplementary data

Supplementary data to this article can be found online at https://doi.org/10.1016/j.quascirev.2025.109727.

Data availability

Proxy and climate reconstruction data available at https://doi.org/10.6084/m9.figshare.30000991.

References

Ajallooeian, F., Dubois, N., Ladd, S.N., Lever, M., Schubert, C.J., De Jonge, C., 2024. Controls on Brgdgt Distributions in the Suspended Particulate Matter of the Seasonally Anoxic Water Column of Rotsee. EGUsphere. https://doi.org/10.5194/egusphere-2024-3052.

Alley, R., Agustsdottir, A., 2005. The 8 K event: cause and consequences of a major Holocene abrupt climate change. Quat. Sci. Rev. 24, 1123–1149. https://doi.org/10.1016/j.quascirev.2004.12.004.

Alley, R.B., Mayewski, P.A., Sowers, T., Stuiver, M., Taylor, K.C., Clark, P.U., 1997. Holocene climatic instability: a prominent, widespread event 8200 yr ago. Geology 25, 483–486. https://doi.org/10.1130/0091-7613(1997)025<0483:HCIAPW>2.3.CO, 2.

Bakkelund, A., Porter, T.J., Froese, D.G., Feakins, S.J., 2018. Net fractionation of hydrogen isotopes in *n*-alkanoic acids from soils in the northern boreal forest. Org. Geochem. 125, 1–13. https://doi.org/10.1016/j.orggeochem.2018.08.005.

Bauersachs, T., Schubert, C.J., Mayr, C., Gilli, A., Schwark, L., 2024. Branched GDGT-based temperature calibrations from Central European lakes. Sci. Total Environ. 906, 167724. https://doi.org/10.1016/j.scitotenv.2023.167724.

Berggren, G., 1981. Atlas of seeds and small fruits of Northwest-European plant species: (sweden, Norway, Denmark, East Fennoscandia and Iceland): with morphological descriptions. Pt 3: Salicaceae - Cruciferae. In: Swedish Museum of Natural History. Stockholm.

Birks, H.J.B., Braak, C.J.F.T., Line, J.M., Juggins, S., Stevenson, A.C., 1990. Diatoms and pH reconstruction. Philos. Trans. R. Soc. Lond. B Biol. Sci. 327, 263–278. https://doi.org/10.1098/rstb.1990.0062.

Birks, H.H., 2013. Plant macrofossil introduction. In: Elias, S.A., Mock, C.J. (Eds.), Encyclopedia of Quaternary Science, second ed. Elsevier, Amsterdam, pp. 593–612. https://doi.org/10.1016/B978-0-444-53643-3.00203-X.

Birks, H.H., 2002. Plant macrofossils. In: Smol, J.P., Birks, H.J.B., Last, W.M., Bradley, R. S., Alverson, K. (Eds.), Tracking Environmental Change Using Lake Sediments, Developments in Paleoenvironmental Research. Springer, Netherlands, Dordrecht, pp. 49–74. https://doi.org/10.1007/0-306-47668-14.

Birks, H.H., Birks, H.J.B., 2000. Future uses of pollen analysis must include plant macrofossils. J. Biogeogr. 27, 31–35. https://doi.org/10.1046/j.1365-2699.2000.00375.x.

Birks, H.J.B., Heiri, O., Seppä, H., Bjune, A.E., 2011. Strengths and weaknesses of quantitative climate reconstructions based on late-quaternary biological proxies. Open Ecol. J. 3, 68–110. https://doi.org/10.1016/j.quaint.2012.07.228.

Bjune, A.E., Birks, H.J.B., Seppä, H., 2004. Holocene vegetation and climate history on a Continental-Oceanic transect in northern Fennoscandia based on pollen and plant macrofossils. Boreas 33, 211–223. https://doi.org/10.1111/j.1502-3885.2004.tb01142.x.

Blaauw, M., Christen, J.A., 2011. Flexible paleoclimate age-depth models using an autoregressive gamma process. Bayesian Analysis 6, 457–474. https://doi.org/10.1214/11-BA618.

Blaauw, M., Christen, J.A., Bennett, K.D., Reimer, P.J., 2018. Double the dates and go for Bayes—Impacts of model choice, dating density and quality on chronologies. Quat. Sci. Rev. 188, 58–66. https://doi.org/10.1016/j.quascirev.2018.03.032.

Bond, G., Showers, W., Cheseby, M., Lotti, R., Almasi, P., deMenocal, P., Priore, P., Cullen, H., Hajdas, I., Bonani, G., 1997. A pervasive millennial-scale cycle in north Atlantic Holocene and glacial climates. Science 278, 1257–1266. https://doi.org/10.1126/science.278.5341.1257.

Bradley, R.B., 2014. Paleoclimatology. Reconstructing Climates of the Quaternary. Elsevier Academic Press.

Breiman, L., 2001. Random forests. Mach. Learn. 45, 5–32. https://doi.org/10.1023/A:1010933404324.

Cañellas-Boltà, N., Rull, V., Sáez, A., Margalef, O., Giralt, S., Pueyo, J.J., Birks, H.H., Birks, H.J.B., Pla-Rabes, S., 2012. Macrofossils in Raraku Lake (Easter Island) integrated with sedimentary and geochemical records: towards a palaeoecological synthesis for the last 34,000 years. Quat. Sci. Rev. 34, 113–126. https://doi.org/10.1016/j.quascirev.2011.12.013.

Cao, J., Rao, Z., Shi, F., Jia, G., 2020. Ice formation on lake surfaces in winter causes warm-season bias of lacustrine brGDGT temperature estimates. Biogeosciences 17, 2521–2536. https://doi.org/10.5194/bg-17-2521-2020.

Cappers, R.T., Bekker, R.M., Jans, J.E., 2012. Digital seed atlas of the Netherlands. Barkhuis.

Chamberlain, S.A., Boettiger, C., 2017. R Python, and Ruby clients for GBIF species occurrence data. PeerJ 5. https://doi.org/10.7287/peerj.preprints.3304v1 e3304vl.

Chevalier, M., 2022. *Crestr*: an R package to perform probabilistic climate reconstructions from palaeoecological datasets. Clim. Past 18, 821–844. https://doi.org/10.5194/cp-18-821-2022.

Clark, P.U., Marshall, S.J., Clarke, G.K.C., Hostetler, S.W., Licciardi, J.M., Teller, J.T., 2001. Freshwater forcing of abrupt climate change during the last glaciation. Science 293, 283–287. https://doi.org/10.1126/science.1062517.

Cremer, H., Andreev, Andrei, Hubberten, Hans-Wolfgang, Wischer, F., 2004. Paleolimnological reconstructions of Holocene environments and climate from Lake Lyadhej-To, ural Mountains, Northern Russia. Arctic Antarct. Alpine Res. 36, 147–155. https://doi.org/10.1657/1523-0430(2004)036[0147:PROHEA]2.0.CO;2.

Damsté, J.S.S., Ossebaar, J., Abbas, B., Schouten, S., Verschuren, D., 2009. Fluxes and distribution of tetraether lipids in an equatorial African lake: constraints on the application of the TEX86 palaeothermometer and BIT index in lacustrine settings. Geochem. Cosmochim. Acta 73, 4232–4249. https://doi.org/10.1016/j.gca.2009.04.022.

Dang, X., Xue, J., Yang, H., Xie, S., 2016. Environmental impacts on the distribution of microbial tetraether lipids in Chinese lakes with contrasting pH: implications for lacustrine paleoenvironmental reconstructions. Sci. China Earth Sci. 59, 939–950. https://doi.org/10.1007/s11430-015-5234-z.

De Jonge, C., Hopmans, E.C., Zell, C.I., Kim, J.-H., Schouten, S., Damsté, J.S.S., 2014. Occurrence and abundance of 6-methyl branched glycerol dialkyl glycerol tetraethers in soils: implications for palaeoclimate reconstruction. Geochem. Cosmochim. Acta 141, 97–112. https://doi.org/10.1016/j.gca.2014.06.013.

De'ath, G., 2007. Boosted trees for ecological modeling and prediction. Ecology 88, 243–251. https://doi.org/10.1890/0012-9658 (2007)88[243:BTFEMA]2.0.CO;2.

De'ath, G., Fabricius, K.E., 2000. Classification and regression trees: a powerful yet simple technique for ecological data analysis. Ecology 81, 3178–3192. https://doi.org/10.1890/0012-9658(2000)081[3178:CARTAP]2.0.CO;2.

Ding, S., Xu, Y., Wang, Y., He, Y., Hou, J., Chen, L., He, J.-S., 2015. Distribution of branched glycerol dialkyl glycerol tetraethers in surface soils of the Qinghai–Tibetan Plateau: implications of brGDGTs-based proxies in cold and dry regions. Biogeosciences 12, 3141–3151. https://doi.org/10.5194/bg-12-3141-2015.

Eldevik, T., Risebrobakken, B., Bjune, A.E., Andersson, C., Birks, H.J.B., Dokken, T.M., Drange, H., Glessmer, M.S., Li, C., Nilsen, J.E.Ø., Otterå, O.H., Richter, K., Skagseth, Ø., 2014. A brief history of climate – the northern seas from the Last Glacial Maximum to global warming. Quat. Sci. Rev. 106, 225–246. https://doi.org/10.1016/j.quascirev.2014.06.028.

Finnish Environmental Center, 2020. Vegetation Zones and Biogeographic Zones. Finnish Environment Institute, Syke, Helsinki, Finland. https://ckan.ymparisto.fi/dataset/kasvillisuusvyohykkeet-ja-luonnonmaantieteelliset-vyohykkeet.

Finnish Meteorological Institute, 2024. Ilmastokatsaus-Digilehti Huhtikuu 2024 | Ilmastokatsaus – Ilmatieteen Laitos. Ilmastokatsaus 24.

Finnish Meteorological Institute, 2022. Finnish Meteorological Institute. https://en.ilmatieteenlaitos.fi/statistics-from-1961-onwards (accessed 9.7.22).

GBIF.org, 2024. GBIF Occurrence Download. https://doi.org/10.15468/dl.b36z2y.

GRASS Development Team, 2024. Geographic Resources Analysis Support System (GRASS) Software.

Harbert, R.S., Baryiames, A.A., 2020. cRacle: r tools for estimating climate from vegetation. Applications in Plant Sciences 8, e11322. https://doi.org/10.1002/aps3.11322.

Heiri, O., Lotter, A.F., Lemcke, G., 2001. Loss on ignition as a method for estimating organic and carbonate content in sediments: reproducibility and comparability of results. J. Paleolimnol. 25, 101–110. https://doi.org/10.1023/A:1008119611481.

Helama, S., Jones, P.D., Briffa, K.R., 2017. Dark ages cold period: a literature review and directions for future research. Holocene 27, 1600–1606. https://doi.org/10.1177/0959683617693898.

Hersbach, H., Bell, B., Berrisford, P., Hirahara, S., Horányi, A., Muñoz-Sabater, J., Nicolas, J., Peubey, C., Radu, R., Schepers, D., Simmons, A., Soci, C., Abdalla, S., Abellan, X., Balsamo, G., Bechtold, P., Biavati, G., Bidlot, J., Bonavita, M., De Chiara, G., Dahlgren, P., Dee, D., Diamantakis, M., Dragani, R., Flemming, J., Forbes, R., Fuentes, M., Geer, A., Haimberger, L., Healy, S., Hogan, R.J., Hólm, E., Janisková, M., Keeley, S., Laloyaux, P., Lopez, P., Lupu, C., Radnoti, G., De Rosnay, P., Rozum, I., Vamborg, F., Villaume, S., Thépaut, J., 2020. The ERA5 global reanalysis. Q. J. R. Meteorol. Soc. 146, 1999–2049. https://doi.org/10.1002/qj.3803.

Holtzman, H., Thomas, E.K., Erb, M., Marshall, L., Castañeda, I.S., Kaufman, D., McKay, N.P., Melles, M., 2025. Early Holocene atmospheric circulation changes over Northern Europe based on isotopic and biomarker evidence from Kola peninsula. Paleoceanogr. Paleoclimatol. 40. https://doi.org/10.1029/2024PA005076 e2024PA005076.

Hopmans, E.C., Schouten, S., Sinninghe Damsté, J.S., 2016. The effect of improved chromatography on GDGT-based palaeoproxies. Org. Geochem. 93, 1–6. https://doi.org/10.1016/j.orggeochem.2015.12.006.

IPCC, 2007. Climate Change 2007: the Physical Science Basis Summary for Policymakers. Cambridge University Press, Cambridge, UK and New York, USA.

Isarin, R.F.B., Bohncke, S.J.P., 1999. Mean July temperatures during the younger dryas in Northwestern and central Europe as inferred from climate indicator plant species. Quat. Res. 51, 158–173. https://doi.org/10.1006/qres.1998.2023.

Jowsey, P.C., 1966. An improved peat sampler. New Phytol. 65, 245–248. https://doi.org/10.1111/j.1469-8137.1966.tb06356.x.

Juggins, S., 2024. Rioja: analysis of Quaternary Science Data, R. package version (1.0-7). https://cran.r-project.org/package=rioja.

Juggins, S., Birks, H.J.B., 2012. Quantitative environmental reconstructions from biological data. In: Birks, H.J.B., Lotter, A.F., Juggins, S., Smol, J.P. (Eds.), Tracking Environmental Change Using Lake Sediments: Data Handling and Numerical Techniques. Springer, Netherlands, Dordrecht, pp. 431–494. https://doi.org/10.1007/978-94-007-2745-8_14.

Kassambara, A., Mundt, F., 2020. Factoextra: Extract and Visualize the Results of Multivariate Data Analyses, R. Package Version (1.0.7). https://doi.org/10.32614/CRAN.package factoextra.

Kaufman, D., McKay, N., Routson, C., Erb, M., Dätwyler, C., Sommer, P.S., Heiri, O., Davis, B., 2020. Holocene global mean surface temperature, a multi-method reconstruction approach. Sci. Data 7, 201. https://doi.org/10.1038/s41597-020-0530-7.

Krikunova, A.I., Kostromina, N.A., Savelieva, L.A., Tolstobrov, D.S., Petrov, A.Y., Long, T., Kobe, F., Leipe, C., Tarasov, P.E., 2022. Late- and postglacial vegetation and climate history of the central Kola Peninsula derived from a radiocarbon-dated pollen record of Lake Kamenistoe. Palaeogeogr. Palaeoclimatol. Palaeoecol. 603, 111191. https://doi.org/10.1016/j.palaeo.2022.111191.

Kuang, X., Schenk, F., Smittenberg, R., Hällberg, P., Zhang, Q., 2021. Seasonal evolution differences of east Asian summer monsoon precipitation between Bølling-Allerød and younger Dryas periods. Clim. Change 165, 19. https://doi.org/10.1007/s10584-021-03025-z.

Laskar, J., Robutel, P., Joutel, F., Gastineau, M., Correia, A.C.M., Levrard, B., 2004. A long-term numerical solution for the insolation quantities of the Earth. Astron. Astrophys. 428, 261–285. https://doi.org/10.1051/0004-6361:20041335.

Lenz, M., Savelieva, L., Frolova, L., Cherezova, A., Moros, M., Baumer, M.M., Gromig, R., Kostromina, N., Nigmatullin, N., Kolka, V., Wagner, B., Fedorov, G., Melles, M., 2021. Lateglacial and Holocene environmental history of the central Kola region, northwestern Russia revealed by a sediment succession from Lake Imandra. Boreas 50, 76–100. https://doi.org/10.1111/bor.12465.

Liang, J., Chevalier, M., Liu, K., Perfumo, A., Wang, M., Xie, H., Hou, J., Herzschuh, U., Chen, F., 2024. Discrepancies in lacustrine bacterial lipid temperature reconstructions explained by microbial ecology. Commun. Earth Environ. 5, 1–14. https://doi.org/10.1038/s43247-024-01925-3.

Liaw, A., Wiener, M., 2002. Classification and regression by randomForest. R. News 2, 18–22.

Loomis, S.E., Russell, J.M., Heureux, A.M., D'Andrea, W.J., Damsté, J.S.S., 2014. Seasonal variability of branched glycerol dialkyl glycerol tetraethers (brGDGTs) in a temperate lake system. Geochem. Cosmochim. Acta 144, 173–187. https://doi.org/10.1016/j.gca.2014.08.027.

Luoto, T.P., Kaukolehto, M., Weckström, J., Korhola, A., Väliranta, M., 2014. New evidence of warm early-holocene summers in subarctic Finland based on an enhanced regional chironomid-based temperature calibration model. Quaternary Resesearch 81, 50–62. https://doi.org/10.1016/j.yqres.2013.09.010.

Maechler, M., 2018. Cluster: cluster analysis basics and extensions. https://CRAN.R-project.org/package=cluster.

Mann, M.E., Zhang, Z., Rutherford, S., Bradley, R.S., Hughes, M.K., Shindell, D., Ammann, C., Faluvegi, G., Ni, F., 2009. Global signatures and dynamical origins of the little ice Age and medieval climate anomaly. Science 326, 1256–1260. https://doi.org/10.1126/science.1177303.

Martínez-Sosa, P., Tierney, J.E., Meredith, L.K., 2020. Controlled lacustrine microcosms show a brGDGT response to environmental perturbations. Org. Geochem. 145, 104041. https://doi.org/10.1016/j.orggeochem.2020.104041.

Martínez-Sosa, P., Tierney, J.E., Pérez-Angel, L.C., Stefanescu, I.C., Guo, J., Kirkels, F., Sepúlveda, J., Peterse, F., Shuman, B.N., Reyes, A.V., 2023. Development and application of the branched and isoprenoid GDGT machine learning classification Algorithm (BIGMaC) for paleoenvironmental reconstruction. Paleoceanogr. Paleoclimatol. 38. https://doi.org/10.1029/2023PA004611 e2023PA004611.

Martínez-Sosa, P., Tierney, J.E., Stefanescu, I.C., Crampton-Flood, E.D., Shuman, B.N., Routson, C., 2021. A global Bayesian temperature calibration for lacustrine brGDGTs. Geochem. Cosmochim. Acta 305, 87–105. https://doi.org/10.1016/j.gca.2021.04.038.

Mateo-Beneito, A., Florescu, G., Tátosová, J., Carter, V.A., Chiverrell, R., Heiri, O., Vasiliev, I., Kuosmanen, N., Kuneš, P., 2024. Multi-proxy temperature and environmental reconstruction during the Late Glacial and Early Holocene in the Bohemian Forest, Central Europe. Quat. Sci. Rev. 331, 108647. https://doi.org/10.1016/j.quascirev.2024.108647.

Mauquoy, D., Van Geel, B., 2013. Plant macrofossil methods and studies: mire and peat macros. In: Encyclopedia of Quaternary Science. Elsevier Inc., pp. 637–656

Miller, D.R., Habicht, M.H., Keisling, B.A., Castañeda, I.S., Bradley, R.S., 2018. A 900-year New England temperature reconstruction from in situ seasonally produced branched glycerol dialkyl glycerol tetraethers (brGDGTs). Clim. Past 14, 1653–1667. https://doi.org/10.5194/cp-14-1653-2018.

Miller, G.H., Brigham-Grette, J., Alley, R.B., Anderson, L., Bauch, H.A., Douglas, M.S.V., Edwards, M.E., Elias, S.A., Finney, B.P., Fitzpatrick, J.J., Funder, S.V., Herbert, T.D., Hinzman, L.D., Kaufman, D.S., MacDonald, G.M., Polyak, L., Robock, A., Serreze, M.C., Smol, J.P., Spielhagen, R., White, J.W.C., Wolfe, A.P., Wolff, E.W., 2010. Temperature and precipitation history of the Arctic. Quat. Sci. Rev. 29, 1679–1715. https://doi.org/10.1016/j.quascirev.2010.03.001.

Moore, P.D., Webb, J.A., Collinson, M.E., 1991. Pollen Analysis, second ed. Blackwell Scientific Publications, London.

Muñoz, S.E., Porter, T.J., Bakkelund, A., Nusbaumer, J., Dee, S.G., Hamilton, B., Giosan, L., Tierney, J.E., 2020. Lipid biomarker record documents hydroclimatic variability of the Mississippi River Basin during the common era. Geophys. Res. Lett. 47. https://doi.org/10.1029/2020GL087237 e2020GL087237.

National Land Survey of Finland, 2014. Elevation model 2 m. Geographic location – entire Finland. https://www.maanmittauslaitos.fi/en/maps-and-spatial-data/datasets-and-interfaces/product-descriptions/elevation-model-2-m.

New, M., Lister, D., Hulme, M., Makin, I., 2002. A high-resolution data set of surface climate over global land areas. Clim. Res. 21, 1–25. https://doi.org/10.3354/cr021001.

Novak, J.B., Russell, J.M., Lindemuth, E.R., Prokopenko, A.A., Pérez-Angel, L., Zhao, B., Swann, G.E.A., Polissar, P.J., 2025. The Branched GDGT isomer Ratio refines lacustrine paleotemperature estimates. G-cubed 26. https://doi.org/10.1029/2024GC012069 e2024GC012069.

Otiniano, G.A., Porter, T.J., Buceta, R.E., Bergman, M.E., Phillips, M.A., 2023. Climatic and environmentally driven variability in lacustrine brGDGT distributions at local to regional scales in Alaska and northwestern Canada. Org. Geochem. 181, 104604. https://doi.org/10.1016/j.orggeochem.2023.104604.

Otiniano, G.A., Porter, T.J., Phillips, M.A., Juutinen, S., Weckström, J.B., Heikkilä, M.P., 2024. Reconstructing warm-season temperatures using brGDGTs and assessing biases in Holocene temperature records in northern Fennoscandia. Quat. Sci. Rev. 329, 108555. https://doi.org/10.1016/j.quascirev.2024.108555.

Overpeck, J.T., Iii, T.W., Prentice, I.C., 1985. Quantitative interpretation of fossil Pollen spectra: dissimilarity coefficients and the method of modern analogs. Quat. Res. 23, 87–108. https://doi.org/10.1016/0033-5894(85)90074-2.

Pearson, E.J., Juggins, S., Talbot, H.M., Weckström, J., Rosén, P., Ryves, D.B., Roberts, S.J., Schmidt, R., 2011. A lacustrine GDGT-temperature calibration from the Scandinavian Arctic to Antarctic: renewed potential for the application of GDGT-paleothermometry in lakes. Geochem. Cosmochim. Acta 75, 6225–6238. https://doi.org/10.1016/j.gca.2011.07.042.

Qian, S., Yang, H., Dong, C., Wang, Y., Wu, J., Pei, H., Dang, X., Lu, J., Zhao, S., Xie, S., 2019. Rapid response of fossil tetraether lipids in lake sediments to seasonal environmental variables in a shallow lake in central China: implications for the use of tetraether-based proxies. Org. Geochem. 128, 108–121. https://doi.org/10.1016/j.orggeochem.2018.12.007.

R Core Team, 2023. R: a Language and Environment for Statistical Computing.

Raberg, J.H., de Wet, G.A., Geirsdóttir, Á., Sepúlveda, J., Miller, G.H., 2025. Oxygen depletion in Lake waters May skew brGDGT-Inferred temperatures by more than 10°C. Geophys. Res. Lett. 52. https://doi.org/10.1029/2024GL113562 e2024GL113562.

Raberg, J.H., Harning, D.J., Crump, S.E., de Wet, G., Blumm, A., Kopf, S., Geirsdóttir, Á., Miller, G.H., Sepúlveda, J., 2021. Revised fractional abundances and warm-season temperatures substantially improve brGDGT calibrations in lake sediments. Biogeosciences 18, 3579–3603. https://doi.org/10.5194/bg-18-3579-2021.

Raberg, J.H., Miller, G.H., Geirsdóttir, Á., Sepúlveda, J., 2022. Near-universal trends in brGDGT lipid distributions in nature. Sci. Adv. 8. https://doi.org/10.1126/sciadv.abm7625 eabm7625.

Rasmussen, S.O., Vinther, B.M., Clausen, H.B., Andersen, K.K., 2007. Early Holocene climate oscillations recorded in three Greenland ice cores. Quat. Sci. Rev. 26, 1907–1914. https://doi.org/10.1016/j.quascirev.2007.06.015.

Reille, M., 1992. Pollen Et Spores D'Europe Et D'Afrique Du Nord. Laboratoire de Botanique Historique et Palynologie, Marseille, France.

Reimer, P.J., Austin, W.E.N., Bard, E., Bayliss, A., Blackwell, P.G., Ramsey, C.B., Butzin, M., Cheng, H., Edwards, R.L., Friedrich, M., Grootes, P.M., Guilderson, T.P., Hajdas, I., Heaton, T.J., Hogg, A.G., Hughen, K.A., Kromer, B., Manning, S.W., Muscheler, R., Palmer, J.G., Pearson, C., Plicht, J. van der, Reimer, R.W., Richards, D.A., Scott, E.M., Southon, J.R., Turney, C.S.M., Wacker, L., Adolphi, F., Büntgen, U., Capano, M., Fahrni, S.M., Fogtmann-Schulz, A., Friedrich, R., Köhler, P., Kudsk, S., Miyake, F., Olsen, J., Reinig, F., Sakamoto, M., Sookdeo, A., Talamo, S., 2020. The IntCal20 Northern hemisphere radiocarbon Age calibration curve (0–55 cal kBP). Radiocarbon 62, 725–757. https://doi.org/10.1017/RDC.2020.41.

Renssen, H., Seppä, H., Crosta, X., Goosse, H., Roche, D.M., 2012. Global characterization of the Holocene Thermal Maximum. Quat. Sci. Rev. 48, 7–19. https://doi.org/10.1016/j.quascirev.2012.05.022.

Renssen, H., Seppä, H., Heiri, O., Roche, D.M., Goosse, H., Fichefet, T., 2009. The spatial and temporal complexity of the Holocene thermal maximum. Nat. Geosci. 2, 411–414. https://doi.org/10.1038/ngeo513.

Ridgeway, G., 2020. Gbm: generalized boosted regression models. https://CRAN.R-project.org/package=gbm.

Russell, J.M., Hopmans, E.C., Loomis, S.E., Liang, J., Sinninghe Damsté, J.S., 2018. Distributions of 5- and 6-methyl branched glycerol dialkyl glycerol tetraethers (brGDGTs) in East African lake sediment: effects of temperature, pH, and new lacustrine paleotemperature calibrations. Org. Geochem. 117, 56–69. https://doi.org/10.1016/j.orggeochem.2017.12.003.

Salonen, J.S., Helmens, K.F., Brendryen, J., Kuosmanen, N., Väliranta, M., Goring, S., Korpela, M., Kylander, M., Philip, A., Plikk, A., 2018. Abrupt high-latitude climate events and decoupled seasonal trends during the Eemian. Nat. Commun. 9, 2851. https://doi.org/10.1038/s41467-018-05314-1.

Salonen, J.S., Helmens, K.F., Seppä, H., Birks, H.J.B., 2013. Pollen-based palaeoclimate reconstructions over long glacial–interglacial timescales: methodological tests based on the Holocene and MIS 5d–c deposits at Sokli, northern Finland. J. Quat. Sci. 28, 271–282. https://doi.org/10.1002/jqs.2611.

Salonen, J.S., Korpela, M., Williams, J.W., Luoto, M., 2019. Machine-learning based reconstructions of primary and secondary climate variables from North American and European fossil pollen data. Sci. Rep. 9, 15805. https://doi.org/10.1038/s41598-019-52293-4.

Salonen, J.S., Kuosmanen, N., Alsos, I.G., Heintzman, P.D., Rijal, D.P., Schenk, F., Bogren, F., Luoto, M., Philip, A., Piilo, S., Trasune, L., Väliranta, M., Helmens, K.F., 2024. Uncovering Holocene climate fluctuations and ancient conifer populations: insights from a high-resolution multi-proxy record from Northern Finland. Global Planet. Change 237, 104462. https://doi.org/10.1016/j.gloplacha.2024.104462.

Salonen, J.S., Schenk, F., Williams, J.W., Shuman, B., Lindroth Dauner, A.L., Wagner, S., Jungclaus, J., Zhang, Q., Luoto, M., 2025. Patterns and drivers of Holocene moisture variability in mid-latitude eastern North America. Nat. Commun. 16, 3582. https://doi.org/10.1038/s41467-025-58685-7.

Schenk, F., Wohlfarth, B., 2019. The imprint of hemispheric-scale climate transitions on the European climate during the last deglaciation (15.5 ka to 9 ka BP). Svensk Kärnbränslehantering AB. In: Swedish Nuclear Fuel and Waste Management Company. Sweden.

Schouten, S., Hopmans, E.C., Sinninghe Damsté, J.S., 2013. The organic geochemistry of glycerol dialkyl glycerol tetraether lipids: a review. Org. Geochem. 54, 19–61. https://doi.org/10.1016/j.orggeochem.2012.09.006.

Sejrup, H.P., Seppä, H., McKay, N.P., Kaufman, D.S., Geirsdóttir, Á., de Vernal, A., Renssen, H., Husum, K., Jennings, A., Andrews, J.T., 2016. North Atlantic-Fennoscandian Holocene climate trends and mechanisms. Quat. Sci. Rev. 147, 365–378. https://doi.org/10.1016/j.quascirev.2016.06.005.

Seppä, H., Birks, H.H., Birks, H.J.B., 2002. Rapid climatic changes during the Greenland stadial 1 (Younger Dryas) to early Holocene transition on the Norwegian Barents Sea Coast. Boreas 31, 215–225. https://doi.org/10.1111/j.1502-3885.2002.tb01068.x.

Seppä, H., Bjune, A.E., Telford, R.J., Birks, H.J.B., Veski, S., 2009. Last nine-thousand years of temperature variability in Northern Europe. Clim. Past 5, 523–535. https://doi.org/10.5194/cp-5-523-2009.

Seppä, H., MacDonald, G.M., Birks, H.J.B., Gervais, B.R., Snyder, J.A., 2008. Late-Quaternary summer temperature changes in the northern-european tree-line region. Quat. Res. 69, 404–412. https://doi.org/10.1016/j.yqres.2008.02.002.

Shala, S., Helmens, K.F., Luoto, T.P., Salonen, J.S., Väliranta, M., Weckström, J., 2017. Comparison of quantitative Holocene temperature reconstructions using multiple proxies from a northern boreal lake. Holocene 27, 1745–1755. https://doi.org/10.1177/0959683617708442.

Sheinkman, V., Sedov, S., Shumilovskikh, L., Korkina, E., Korkin, S., Zinovyev, E., Golyeva, A., 2016. First results from the Late Pleistocene paleosols in northern Western Siberia: implications for pedogenesis and landscape evolution at the end of MIS3. Quat. Int. 418, 132–146. https://doi.org/10.1016/j.quaint.2015.12.095.

Simpson, G.L., 2018. Modelling palaeoecological time series using generalised additive models. Front. Ecol. Evol. 6. https://doi.org/10.3389/fevo.2018.00149.

Sjögren, P.J.E., 2021. An overview of Holocene climate reconstructions in northernmost Fennoscandia: a contribution to the Stone Age demographics project. Septentrio Reports. https://doi.org/10.7557/7.5747.

Stefanescu, I.C., Shuman, B.N., Tierney, J.E., 2021. Temperature and water depth effects on brGDGT distributions in sub-alpine lakes of mid-latitude North America. Org. Geochem. 152, 104174. https://doi.org/10.1016/j.orggeochem.2020.104174.

Sweeney, C.A., 2004. A key for the identification of stomata of the native conifers of Scandinavia. Rev. Palaeobot. Palynol. 128, 281–290. https://doi.org/10.1016/S0034-6667(03)00138-6.

ter Braak, C.J.F., Juggins, S., 1993. Weighted averaging partial least squares regression (WA-PLS): an improved method for reconstructing environmental variables from species assemblages. In: van Dam, H. (Ed.), Twelfth International Diatom Symposium. Springer, Netherlands, Dordrecht, pp. 485–502. https://doi.org/10.1007/978-94-017-3622-0_49.

Trasune, L., Väliranta, M., Stivrins, N., Amon, L., Schenk, F., Salonen, J.S., 2024. A comparison of plant macrofossil-based quantitative climate reconstruction methods: a case study of the lateglacial Baltic States. Quat. Sci. Rev. 338, 108811. https://doi.org/10.1016/j.quascirev.2024.108811.

Väliranta, M., Salonen, J.S., Heikkilä, M., Amon, L., Helmens, K., Klimaschewski, A., Kuhry, P., Kultti, S., Poska, A., Shala, S., Veski, S., Birks, H.H., 2015. Plant macrofossil evidence for an early onset of the Holocene summer thermal maximum in northernmost Europe. Nature Communundications 6, 6809. https://doi.org/10.1038/ncomms7809.

Wang, H., Chen, W., Zhao, H., Cao, Y., Hu, J., Zhao, Z., Cai, Z., Wu, S., Liu, Z., Liu, W., 2023. Biomarker-based quantitative constraints on maximal soil-derived brGDGTs in modern lake sediments. Earth Planet Sci. Lett. 602, 117947. https://doi.org/10.1016/j.epsl.2022.117947.

Wang, H., Liu, Z., Zhao, H., Cao, Y., Hu, J., Lu, H., Zhao, Z., Cai, Z., Liu, X., Liu, W., 2024. New calibration of terrestrial brGDGT paleothermometer deconvolves distinct temperature responses of two isomer sets. Earth Planet Sci. Lett. 626, 118497. https://doi.org/10.1016/j.epsl.2023.118497.

Wanner, H., Beer, J., Bütikofer, J., Crowley, T.J., Cubasch, U., Flückiger, J., Goosse, H., Grosjean, M., Joos, F., Kaplan, J.O., Küttel, M., Müller, S.A., Prentice, I.C., Solomina, O., Stocker, T.F., Tarasov, P., Wagner, M., Widmann, M., 2008. Mid- to late Holocene climate change: an overview. Quat. Sci. Rev. 27, 1791–1828. https://doi.org/10.1016/j.quascirev.2008.06.013.

Wanner, H., Mercolli, L., Grosjean, M., Ritz, S.P., 2015. Holocene climate variability and change; a data-based review. Journal of Geolological Society 172, 254–263. https://doi.org/10.1144/jgs2013-101.

Webb, T., 1986. Is vegetation in equilibrium with climate? How to interpret late-Quaternary pollen data. Vegetatio 67, 75–91. https://doi.org/10.1007/BF00037359.

Weber, Y., De Jonge, C., Rijpstra, W.I.C., Hopmans, E.C., Stadnitskaia, A., Schubert, C.J., Lehmann, M.F., Sinninghe Damsté, J.S., Niemann, H., 2015. Identification and carbon isotope composition of a novel branched GDGT isomer in lake sediments: evidence for lacustrine branched GDGT production. Geochem. Cosmochim. Acta 154, 118–129. https://doi.org/10.1016/j.gca.2015.01.032.

Weijers, J.W., Schouten, S., van den Donker, J.C., Hopmans, E.C., Damsté, J.S.S., 2007. Environmental controls on bacterial tetraether membrane lipid distribution in soils. Geochem. Cosmochim. Acta 71, 703–713. https://doi.org/10.1016/j.gca.2006.10.003.

Weijers, J.W.H., Schouten, S., Hopmans, E.C., Geenevasen, J.A.J., David, O.R.P., Coleman, J.M., Pancost, R.D., Sinninghe Damsté, J.S., 2006. Membrane lipids of mesophilic anaerobic bacteria thriving in peats have typical archaeal traits. Environ. Microbiol. 8, 648–657. https://doi.org/10.1111/j.1462-2920.2005.00941.x.

Wood, S.N., 2017. Generalized Additive Models: an Introduction with R. Chapman and Hall/CRC, United States, p. 496.

Wu, J., Yang, H., Pancost, R.D., Naafs, B.D.A., Qian, S., Dang, X., Sun, H., Pei, H., Wang, R., Zhao, S., Xie, S., 2021. Variations in dissolved O2 in a Chinese lake drive changes in microbial communities and impact sedimentary GDGT distributions. Chem. Geol. 579, 120348. https://doi.org/10.1016/j.chemgeo.2021.120348.

Yao, Y., Zhao, J., Vachula, R.S., Werne, J.P., Wu, J., Song, X., Huang, Y., 2020. Correlation between the ratio of 5-methyl hexamethylated to pentamethylated branched GDGTs (HP5) and water depth reflects redox variations in stratified lakes. Org. Geochem. 147, 104076. https://doi.org/10.1016/j.orggeochem.2020.104076.

Zhao, B., Castañeda, I.S., Bradley, R.S., Salacup, J.M., de Wet, G.A., Daniels, W.C., Schneider, T., 2021. Development of an in situ branched GDGT calibration in Lake 578, southern Greenland. Org. Geochem. 152, 104168. https://doi.org/10.1016/j.orggeochem.2020.104168.

Zhao, B., Russell, J.M., Tsai, V.C., Blaus, A., Parish, M.C., Liang, J., Wilk, A., Du, X., Bush, M.B., 2023. Evaluating global temperature calibrations for lacustrine branched GDGTs: seasonal variability, paleoclimate implications, and future directions. Quat. Sci. Rev. 310, 108124. https://doi.org/10.1016/j.quascirev.2023.108124.

Zhu, Z., Wu, J., Chu, G., Liu, J., 2025. New global lacustrine brGDGTs temperature calibrations based on machine learning. Quat. Sci. Rev. 357, 109319. https://doi.org/10.1016/j.quascirev.2025.109319.

Zhu, Z., Wu, J., Rioual, P., Mingram, J., Yang, H., Zhang, B., Chu, G., Liu, J., 2021. Evaluation of the sources and seasonal production of brGDGTs in lake Sihailongwan (N.E. China) and application to reconstruct paleo-temperatures over the period 60–8 ka BP. Quat. Sci. Rev. 261, 106946. https://doi.org/10.1016/j.quascirev.2021.106946.